Atmos. Chem. Phys., 11, 2503–2536, 2011
www.atmos-chem-phys.net/11/2503/2011/
doi:10.5194/acp-11-2503-2011

Atmospheric Chemistry and Physics

Mesoscale convective systems observed during AMMA and their impact on the NO_x and O_3 budget over West Africa

H. Huntrieser[1], H. Schlager[1], M. Lichtenstern[1], P. Stock[1], T. Hamburger[1], H. Höller[1], K. Schmidt[2], H.-D. Betz[2,3], A. Ulanovsky[4], and F. Ravegnani[5]

[1]Institut für Physik der Atmosphäre, Deutsches Zentrum für Luft- und Raumfahrt (DLR), Oberpfaffenhofen, Germany
[2]nowcast GmbH, München, Germany
[3]Physics Department, University of Munich, Germany
[4]Central Aerological Observatory, Moscow, Russia
[5]Institute of Atmospheric Sciences and Climate (CNR-ISAC), Bologna, Italy

Received: 12 August 2010 – Published in Atmos. Chem. Phys. Discuss.: 5 October 2010
Revised: 23 February 2011 – Accepted: 7 March 2011 – Published: 17 March 2011

Abstract. During the "African Monsoon Multidisciplinary Analysis" (AMMA) field phase in August 2006, a variety of measurements focusing on deep convection were performed over West Africa. The German research aircraft *Falcon* based in Ouagadougou (Burkina Faso) investigated the chemical composition in the outflow of large mesoscale convective systems (MCS). Here we analyse two different types of MCS originating north and south of the intertropical convergence zone (ITCZ, ∼10° N), respectively. In addition to the airborne trace gas measurements, stroke measurements from the Lightning Location Network (LINET), set up in Northern Benin, are analysed. The main focus of the present study is (1) to analyse the trace gas composition (CO, O_3, NO, NO_x, NO_y, and HCHO) in the convective outflow as a function of distance from the convective core, (2) to investigate how different trace gas compositions in the boundary layer (BL) and ambient air may influence the O_3 concentration in the convective outflow, and (3) to estimate the rate of lightning-produced nitrogen oxides per flash in selected thunderstorms and compare it to our previous results for the tropics. The MCS outflow was probed at different altitudes (∼10–12 km) and distances from the convective core (<500 km). Trace gas signatures similar to the conditions in the MCS inflow region were observed in the outflow close to the convective core, due to efficient vertical transport. In the fresh MCS outflow, low O_3 mixing ratios in the range of 35–40 nmol mol^{-1} were observed. Further downwind, O_3 mixing ratios in the outflow rapidly increased with distance, due to mixing with the ambient O_3-rich air. After 2–3 h, O_3 mixing ratios in the range of ∼65 nmol mol^{-1} were observed in the aged outflow. Within the fresh MCS outflow, mean NO_x (=NO + NO_2) mixing ratios were in the range of ∼0.3–0.4 nmol mol^{-1} (peaks ∼1 nmol mol^{-1}) and only slightly enhanced compared to the background. Both lightning-produced NO_x (LNO_x) and NO_x transported upward from the BL contributed about equally to this enhancement. On the basis of Falcon measurements, the mass flux of LNO_x in the investigated MCS was estimated to be ∼100 g(N) s^{-1}. The average stroke rate of the probed thunderstorms was 0.04–0.07 strokes s^{-1} (here only strokes with peak currents ≥10 kA contributing to LNO_x were considered). The LNO_x mass flux and the stroke rate were combined to estimate the LNO_x production rate. For a better comparison with other published results, LNO_x estimates per LINET stroke were scaled to Lightning Imaging Sensor (LIS) flashes. The LNO_x production rate per LIS flash was estimated to 1.0 and 2.5 kg(N) for the MCS located south and north of the ITCZ, respectively. If we assume, that these different types of MCS are typical thunderstorms occurring globally (LIS flash rate ∼44 s^{-1}), the annual global LNO_x production rate was estimated to be ∼1.4 and 3.5 Tg(N) a^{-1}.

Correspondence to: H. Huntrieser
(heidi.huntrieser@dlr.de)

Published by Copernicus Publications on behalf of the European Geosciences Union.

1 Introduction

Deep convection influences the chemical composition in the upper troposphere (UT) in many ways. Strong up- and downdrafts may redistribute trace gases within less than 1 h between the boundary layer (BL) and the UT (Chatfield and Crutzen, 1984; Thompson et al., 1994). Furthermore, the noninductive collisions between small and large ice particles in the presence of supercooled liquid water may initiate lightning (Takahashi, 1978; Saunders et al., 1991). In the hot lightning channel, nitrogen oxide (NO) is one of the most prominent trace gases produced (Chameides et al., 1977; Bhetanabhotla et al., 1985). These processes significantly contribute to change the composition of trace gases in the UT. Within deep convective systems, polluted airmasses with enhanced NO_x ($=NO+NO_2$) content can be transported upward from the BL and mix with airmasses polluted by lightning-produced NO_x (LNO_x) (Dickerson et al., 1987; Bertram et al., 2007). The main global source of NO_x in the UT can be attributed to the latter source, exceeding also the contributions from aircraft emissions and injections from the stratosphere. In a recent review article on LNO_x by Schumann and Huntrieser (2007) (=SH07), the global nitrogen production rate by lightning was given a most likely source strength of 5 ± 3 Tg(N) a^{-1}.

In the presence of NO_x, ozone (O_3) may be produced by photochemical oxidation of hydrocarbons and carbon monoxide (CO) (Crutzen, 1970; Fishman et al., 1979; Pickering et al., 1993; Jacob et al., 1996). In tropical regions, enhanced O_3 production rates have been observed due to the high solar irradiance (Thompson et al., 1997; Sauvage et al., 2005). Several model studies have investigated the overall influence of convective transport on tropospheric O_3 and its precursors (Lelieveld and Crutzen, 1994; Lawrence et al., 2003; Doherty et al., 2005). In tropical regions, the convective uplift of O_3-poor BL air tend to decrease the O_3 burden in the UT. Concurrently, the uplift and mixing of O_3 precursors may increase the O_3 burden. Ozone plays an essential role in atmospheric chemistry since it determines the oxidizing capacity of the troposphere and acts as an important greenhouse gas. To achieve significant progress in the modelling of tropospheric ozone in the future, it is important to better constrain the global and regional source strength of LNO_x emissions, especially in tropical regions (Martin et al., 2002). Recent observations and model results give some indications that values at the lower end of the range given by SH07 for the global LNO_x source strength are more suitable for certain tropical and maritime regions, whereas values in the upper range are more suitable for subtropical and midlatitude continental regions (Martin et al., 2006; Hudman et al., 2007; Huntrieser et al., 2009; Beirle et al., 2010; Bucsela et al., 2010; Jourdain et al., 2010; Ott et al., 2010). Furthermore, comprehensive model studies carried out by Tost et al. (2007) and Barret et al. (2010), on global as well as regional scales, show that large discrepancies between observations and simulations of lightning still exist. Due to the important influence of NO_x on the O_3 production, especially in tropical regions, further detailed investigations on LNO_x in the tropics are needed, as stated recently by Barthe et al. (2010); Bucsela et al. (2010) and Ott et al. (2010).

It is known that most lightning is produced in the tropics (Christian et al., 2003; Zipser et al., 2006), however until recently measurements and quantifications of nitrogen oxides in the fresh outflow of tropical deep convection were rare (e.g., Koike et al., 2007). In the last years, the Deutsches Zentrum für Luft- und Raumfahrt (DLR) conducted (or participated in) several EU-funded airborne field experiments in the tropics focusing on lightning-produced NO_x, as the "Tropical Convection, Cirrus, and Nitrogen Oxides Experiment" (TROCCINOX) in Brazil in 2004 and 2005, and "Stratospheric-Climate links with Emphasis on the Upper Troposphere and Lower Stratosphere" (SCOUT-O3) in Northern Australia in 2005 (Huntrieser et al., 2007, 2008, 2009; Höller et al., 2009). Here we focus on the most recent one of these tropical field campaigns, the African Monsoon Multidisciplinary Analysis (AMMA) 2006 wet season experiment (Redelsperger et al., 2006). AMMA is an international research program that aims to improve our knowledge and understanding of the West African Monsoon (WAM), and investigates its variability and influence on the regional water resources. In the framework of AMMA, several multidisciplinary field campaigns on multiscales were performed in the past years (Lebel et al., 2009). These are the most detailed measurements of this kind ever performed in this region. One of the key issues was to investigate the largest mesoscale convective systems (MCS) (Houze, 1993, 2004) and their linkage to the WAM variability. The chemical composition of the middle and upper troposphere connected to these deep convective events and their impact on the ozone budget and its precursors over West Africa was a further objective of interest (Ancellet et al., 2009; Bechara et al., 2010).

The DLR participated in the Special Operation Period in August 2006 (SOP-2a2), as reviewed by Reeves et al. (2010), and focused their measurements with the German DLR *Falcon* aircraft on atmospheric chemistry and aerosols in the UT. The main tasks of the DLR were to estimate (1) the chemical and aerosol composition in the outflow of deep convection, and (2) the magnitude of NO_x production by lightning in deep convection over West Africa. In this paper we focus on parts of these two tasks by analysing airborne measurements in the fresh outflow (<12 h). Further analyses of the aged outflow (>12 h) from deep convection are in preparation (H. Schlager, DLR, personal communication, 2010). The main focus of the present study is (1) to analyse the trace gas composition (CO, O_3, NO, NO_x, NO_y, and HCHO) in the convective outflow as a function of distance from the convective core, (2) to investigate how different trace gas compositions in the BL and ambient air may influence the O_3 concentration in the convective outflow, and (3) to estimate the LNO_x production rate per flash in selected

thunderstorms and to compare it to our previous results for the tropics. The measurements performed during AMMA are the first to our knowledge that investigate the NO_x composition in the outflow of West African MCS in more detail by airborne in situ measurements. Up to now, measurements over Africa from satellites and commercial airliners, e.g. within the framework of "Measurements of Ozone, water vapour, carbon monoxide and nitrogen oxides by in-service Airbus aircraft" (MOZAIC), have shown evidence of an important NO_x source from lightning in the UT (e.g., Richter and Burrows, 2002; Sauvage et al., 2005; Sioris et al., 2007). Over the tropical Atlantic and Africa a broad enhancement of $2–6 \times 10^{14}$ molecules NO_2 cm^{-2} has been observed from space and attributed to lightning (Martin et al., 2007).

In addition to the *Falcon* aircraft, we used the Russian M55 *Geophysica* aircraft for trace gas measurements above the convective outflow in the tropical tropopause layer (=TTL, e.g., Highwood and Hoskins, 1998; Fueglistaler et al., 2009; Law et al., 2010). Both aircraft were based in Ouagadougou (12.4° N, 1.5° W) in Burkina Faso during the AMMA SOP-2a2 experiment. Furthermore, the DLR lightning location network (LINET) was set up in the neighbouring state Benin (centred around 10.0° N and 1.5° E). The set up of the airborne trace gas instrumentation and LINET was similar as during TROCCINOX and SCOUT-O3, see Sect. 2. The general meteorological situation during AMMA is described in more detail in Sect. 3, together with a flight summary of two selected cases from 6 and 15 August 2006. In Sect. 4 and in the Appendix A, the method used to analyse the measurements is introduced and discussed in more detail together with some results. The Falcon, Geophysica and LINET measurements are combined and scaled with Lightning Imaging Sensor (LIS) measurements to estimate the LNO_x production rate per LIS flash in the selected thunderstorms, and *to estimate the global annual* LNO_x *production rate based on these different thunderstorms*. The method, which combines the LNO_x *mass flux rate* in the anvil outflow and the *LINET stroke rate*, was already introduced and described in a previous paper by Huntrieser et al. (2008) (=HH08). In Sect. 5, a discussion follows whether mixing with the ambient air or O_3 production changed the O_3 composition in the investigated MCS outflow. Finally, a synthesis of AMMA, SCOUT-O3 and TROCCINOX results concerning LNO_x and recommendations for future LNO_x parameterisations are given in Sects. 6 and 7, respectively. Results from the present study are summarised in Sect. 8.

2 Data

2.1 The AMMA SOP-2a2 campaign

The AMMA project (http://amma-international.org/) was established on a French initiative, built by an international scientific group and supported by the European Community (EC). The AMMA SOP-2a2 campaign, carried out from 25 July to 31 August 2006, involved not only the German *Falcon-20* and Russian M55 *Geophysica* research aircraft based in Ouagadougou, but also the French *Falcon-20* and *ATR-42* aircraft, and the British Facility for Airborne Atmospheric Measurements (FAAM) *BAe-146* aircraft, all based further northeast in Niamey (13.5° N, 2.1° E) in Niger (Mari et al., 2008; Ancellet et al., 2009; Saunois et al., 2009; Bechara et al., 2010; Law et al., 2010; Real et al., 2010; Reeves et al., 2010). Further downstream, in the Cape Verde region off the coast of West Africa, the NASA-AMMA program (NAMMA) examined the interaction between African Easterly waves (AEW) and the Saharan air layer (SAL) and their role in tropical cyclogenesis (Jenkins et al., 2008; Zipser et al, 2009; Cifelli et al., 2010). All of these measurements were mainly performed in August, when the monsoon (wet) season is fully developed. This is the season when the occurrence of large MCS is most prominent and provides most of the annual rainfall (80–90%) to the Sahel zone (10–18° N), located just south of the Sahara (Laurent et al., 1998; Laing et al., 1999; Mathon et al., 2002; Lebel et al., 2003; Zipser et al., 2006; Nieto Ferreira et al., 2009).

2.2 Airborne instrumentation on Falcon and Geophysica, and some trace gas characteristics

In the present study we analyse in situ trace gas measurements carried out by the German *Falcon* in the anvil outflow region of MCS and by the *Geophysica* in the TTL above the main convective outflow. The airborne instrumentation used for this study and the accuracies are listed in Table 1 (see also Andrés-Hernández et al., 2010). The measurements described below in the next subsections are used to investigate the evolution of the trace gas composition in the anvil outflow and to estimate the LNO_x production rate in selected thunderstorm systems in the course of this paper.

In the present study we mainly concentrate on measurements carried out with the Falcon up to ~12 km altitude. The aircraft was equipped with instruments to measure HCHO (formaldehyde), CO, O_3, NO and NO_y mixing ratios and the photolysis rate $J(NO_2)$. The instrumentation has been used during several DLR field campaigns in the past (e.g., Baehr et al., 2003; Huntrieser et al., 2005, 2007, 2009). All instruments (except HCHO) are capable of measuring at high temporal resolution ($\leq$1 s) necessary for investigating the small scale structures in the anvil outflow (Huntrieser et al., 1998, 2002; Höller et al., 1999). The NO_2 (and NO_x) mixing ratios are calculated on the basis of the photostationary steady state equation from the measurements of NO, O_3, $J(NO_2)$, pressure and temperature (Volz-Thomas et al., 1996). The trace gases NO, NO_x, and NO_y were used to investigate both the production by lightning and the convective transport from the BL. During the short timescales of convective transport from the BL to the UT, NO_x is generally conserved but not NO or NO_2 individually. The equilibrium between NO and

Table 1. Airborne instrumentation during AMMA used for the present study.

Aircraft (maximum altitude, km)	Species	Technique	Averaging time, s	Horizontal resolution, m	Accuracy	Principal investigator
Falcon (12 km)	Wind (u, v, w) Temperature Humidity	Rosemount flow angle sensor PT100/Rosemount Composite of dewpoint mirror/ capacitive sensor/Lyman Alpha absorption instrument	1 1 1	∼200	1 m s^{-1} horizontal, 0.3 m s^{-1} vertical 0.5 K	Andreas Giez, DLR, Germany
	O_3	UV absorption	1		5%	Hans Schlager, DLR, Germany
	CO	VUV fluorescence	1		10%	Hans Schlager, DLR, Germany
	NO NO_y	Chemiluminescence	1 1		±1 pmol mol^{-1} ±5 pmol mol^{-1}	Hans Schlager, DLR, Germany
	$J(NO_2)$	Filter radiometry	1		10%	Hans Schlager, DLR, Germany
	HCHO	Hantzsch technique	60		15%	Hans Schlager, DLR, Germany
Geophysica (20 km)	O_3	FOZAN chemiluminescence	1	∼150	±10 nmol mol^{-1}	F. Ravegnani, Consiglio Nazionale delle Richerche (CNR), Bologna, Italy; A. Ulanovski, CAO, Russia

NO_2 is shifted to more NO and less NO_2 in the UT compared to the BL, due to the stronger insolation in the UT. In the MCS outflow region, NO contributes to the major fraction of NO_x with ∼90% and NO_2 only contributes with ∼10%. Compared to the BL, where the lifetime of NO_x is very short (only a few hours), the lifetime in the UT increases to a value of ∼2–3 days (Jacob et al., 1996). Furthermore, due to the high NO_x mixing ratios in the MCS outflow compared to the background it is often possible to trace the MCS outflow for a period of a few days.

The most suitable of these tracers for BL transport is CO, with a lifetime of ∼2–3 months in the troposphere (e.g., Xiao et al., 2007). For fresh transport from the BL, O_3, with a lifetime in the order of days to months, and HCHO, with a short lifetime of 5 h, can partly also be used as tracers (Arlander et al., 1995; Stevenson et al., 2006). Our previous measurements in thunderstorms have shown that the mixing ratios of tracers in the main *outflow* region can occasionally be in the same range as measured at the top of the BL, which indicates a very fast and undiluted vertical transport, a "mirroring" of trace gas compositions (Huntrieser et al., 2002). The main *inflow* region was found to be located at the top of the BL.

In addition to the AMMA Falcon measurements, O_3 measurements up to ∼20 km altitude were obtained from the high-flying Geophysica aircraft (Stefanutti et al., 2004) and used as a general tracer to identify the convective outflow region.

The Falcon aircraft probed the outflow from several, large MCS in the Sahel zone in the vicinity of Burkina Faso. Data from the following MCS missions were selected for further analyses: 1, 4, 6, 7, 11, 15, and 18 August 2006. (During the transfer flights to/from Burkina Faso on 1 and 18 August, only the last/first part of the flights was considered.) Two of the selected flights were analysed in more detail. These were the only flights with available LINET measurements; on 6 August a huge MCS between Niamey and Ouagadougou was probed extensively, and on 15 August (b-flight, second flight of the day) a smaller MCS west of Benin was penetrated several times (see Sect. 3).

The two aircraft were equipped with standard meteorological measurement systems to measure position, altitude, temperature, pressure, horizontal wind velocity and direction. Further instruments on the Falcon measured the relative humidity and the 3-dimensional wind vectors (u, v, w). All flight altitude values refer to pressure height and UTC (Universal Time Coordinated) time. Burkina Faso is located within the UTC time zone.

2.3 Meteorological, lightning, and satellite data

For meteorological analyses, wind and temperature fields based on European Centre for Medium-Range Weather Forecasts (ECMWF) data with a horizontal resolution of 1° × 1° were used (see Sect. 3).

For the observation of lightning, the six-sensors DLR lightning location network LINET was installed in Northern Benin, as described by Höller et al. (2009). This detection system, operating in the very low frequency/low frequency (VLF/LF) (5–200 kHz) range, has been developed by the University of Munich and described in detail by Betz et al. (2004, 2007, 2009), Schmidt et al. (2004, 2005) and

Schmidt (2007). A brief description was recently given by us in HH08 and will therefore not be repeated here. Radiation emitted from both intra-cloud (IC) and cloud-to-ground (CG) sources ("strokes") is detected and the IC emission height is determined. The lightning sensors were located within an area extending from 9.0 to 10.3° N and from 1.1 to 2.7° E. The average distance to the next closest sensor was ∼90 km. Peak currents down to 1–2 kA were measured within the inner region where the detection efficiency was highest; the so-called LINET centre area covering 9.5 to 10.5° N and 1.0 to 2.0° E. However, a decreasing detection efficiency of strokes with low peak currents (<10 kA) with increasing distance from the LINET detection centre has been observed (HH08; Höller et al., 2009). Therefore, for further studies comparing stroke characteristics in different thunderstorms (see Sect. 4) only strokes with peak currents exceeding 10 kA were considered, as already discussed in HH08. In 2005, similar LINET arrays, as for AMMA, were set up in Brazil, Australia and Germany. Recently, the general characteristics of different thunderstorm systems in these three regions were compiled and compared to West African systems (Höller et al., 2009). We also used data from the World Wide Lightning Location Network, WWLLN (e.g. Lay et al., 2004) (http://wwlln.net), to complement the LINET data in a specific case.

In addition, spaceborne measurements from LIS on board the Tropical Rainfall Measurement Mission (TRMM) satellite (Christian et al., 1999; Thomas et al., 2000; Boccippio et al., 2002; Christian and Petersen, 2005) were used to estimate the total regional flash distribution (sum of CG and IC flashes) over the AMMA observation area. For an overview of system characteristics see http://thunder.msfc.nasa.gov/lis/ and a brief description was already given by us in HH08. Here LIS data for one overpass of 14 August 2006 were compared with LINET data (see Sect. 4.5). Our LNO_x estimates per LINET stroke were scaled to LNO_x estimates per LIS flash. Global LIS flash statistics can then be used to provide an estimate of the global strength of the LNO_x production rate.

The cloud development over West Africa was analysed by using infrared (IR) images (see Sect. 3) from Meteosat Second Generation (MSG) operated by the European Organisation for the Exploitation of Meteorological Satellites (EUMETSAT) (http://www.eumetsat.int/).

3 Observations during AMMA

3.1 General meteorological situation and brief chemical characterisation

From July until mid August, the synoptic situation in the AMMA SOP-2a2 observation area was dominated by the WAM (Parker et al., 2005a; Nicholson, 2009). The WAM onset starts with an abrupt latitudinal shift of the intertropical convergence zone (ITCZ) from 5° to 10° N. A detailed meteorological roadmap for the period of the AMMA field experiment has been given by Janicot et al. (2008) and Cairo et al. (2010).

Due to the strong thermal gradient between the heated tropical and subtropical mainland (heat low over the Sahara), and the cooler Gulf of Guinea and South Atlantic Ocean, a pronounced flow from the southwest develops. In August, this onshore monsoon flow reaches its northernmost extent (15–20° N) and displaces the Saharan Air Layer (SAL) at the ground (Lebel et al., 2003). The confluence zone at the surface between this relatively cool, moist southwesterly flow and the hot, dry northeasterly flow from the Sahara (Harmattan) is called the intertropical discontinuity (ITD) or intertropical front (ITF) (Thorncroft and Haile, 1995).

Along the upper transition zone between the monsoon layer and the capping SAL, a pronounced thermal wind develops due to the strong baroclinicity at 3–4 km (600–700 hPa). This midtropospheric jet is known as the African Easterly Jet (AEJ) (Burpee, 1972; Thorncroft et al., 2003). In August, the jet core with 10–15 $m\,s^{-1}$ is located south of the ITD at 10–15° N. The pronounced horizontal and vertical wind shear associated with this jet, as well as the meridional potential vorticity (PV) gradient are crucial parameters for the development and propagation of wave disturbances at 3–4 km altitude (period 3–5 days), known as the African Easterly Waves (AEW) (Burpee, 1972; Cifelli et al., 2010). Furthermore, the vertical shear of the AEJ is essential for the generation of organised long-lived MCS and squall lines that form south of the ITD and propagate rapidly (>10 $m\,s^{-1}$) westwards (Laing and Fritsch, 1993; Mathon et al., 2002). Only these large systems are energetic enough to break through the dry and hot SAL that inhibits convection by capping the monsoon flow (Roca et al., 2005).

In addition to the AEJ, a further jet stream develops in the UT over West Africa in summer, when the ascending branch of the Hadley cell (ITCZ) is located north of the equator. The upper level outflow moving southward to the equator, is in addition enforced by the Coriolis force to move westward, forming the Tropical Easterly Jet (TEJ) (Nicholson, 2009). The jet core at ∼13–14 km (∼150 hPa) with ∼20 $m\,s^{-1}$ is located around 5–10° N in August. Between the TEJ and AEJ (at ∼11° N in August) an extended core of strong ascent is present in the mid- and upper troposphere, which is associated to the major rainbelt of the ITCZ generating long-lived MCS.

The large MCS in the Sahel zone are mainly orographically triggered, preferable over the Jos Plateau in Northern Nigeria (Hodges and Thorncroft, 1997; Laing et al., 2008). Many of the systems are well-organised and fall into the category of mesoscale convective complexes (MCC) (Maddox, 1980). The cloud shields of these systems spread vertically between 10 and 15 km altitude and horizontally over $2–3 \times 10^5$ km^2, and contain a large fraction of trailing stratiform precipitation in addition to the heavy rain in

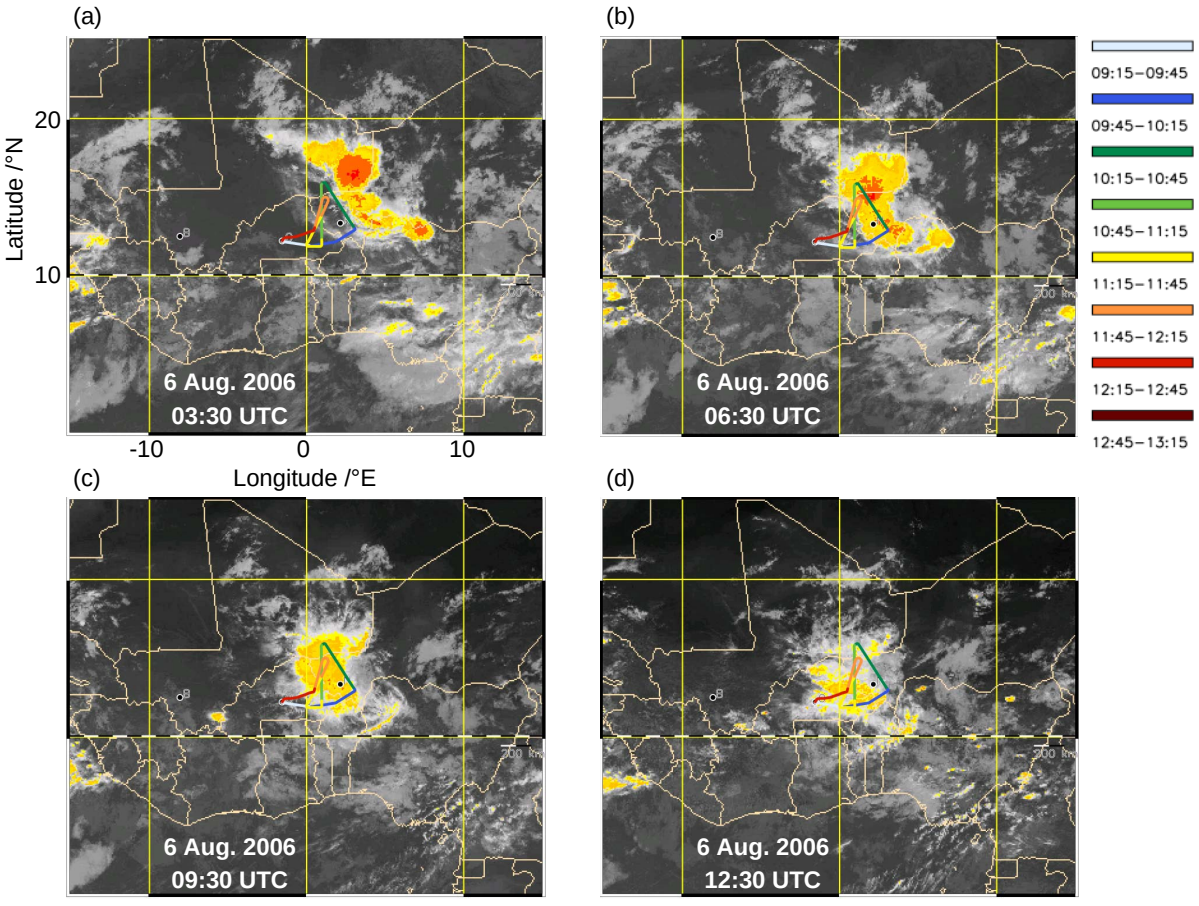

Fig. 1. Meteosat Second Generation (MSG) brightness temperatures over West Africa on 6 August 2006 for 03:30 **(a)**, 06:30 **(b)**, 09:30 **(c)** and 12:30 UTC **(d)** (red 195 K, orange 210 K, yellow 225 K). Superimposed is the Falcon flight track from Ouagadougou in Burkina Faso (colour-coded according to UTC time). The position of the MSC during take-off is indicated in **(c)** and the position during landing in **(d)**. Capital cities of Mali and Niger are indicated with black dots (B = Bamako to the west, N = Niamey to the east).

the convective region. The lifting condensation level (LCL) is especially low during the monsoon season and located at ∼0.5 km (Kollias et al., 2009). The average MCC lifetime is in the range of 12 h, however the largest sized systems may last >24 h (Laing and Fritsch, 1993; Mathon and Laurent, 2001). Global climatologies indicate that a major fraction of the MCS/MCC systems with extensive ice scattering develops over the Sahel zone, Central Africa, Argentina and Southeastern United States (Mohr and Zipser, 1996; Laing and Fritsch, 1997; Houze, 2004).

The general chemical composition of the troposphere during AMMA has been summarised by Reeves et al. (2010). The average vertical profiles of O_3 and CO exhibit "S" and "C"-shapes, respectively. Ozone mixing ratios are especially low in the BL due to photochemical destruction in the humid, monsoon influenced airmasses. Further southward between 6° N and 12° N, also the rapid O_3 deposition over forested areas becomes more important. The rapid uplift of these O_3-poor BL airmasses in deep convection causes a second O_3 minimum in the UT ("S"-shape). Contrarily, O_3 mixing ratios are frequently enhanced in the mid troposphere due to intrusions of airmasses from the Southern Hemisphere impacted by biomass burning and in addition photochemical O_3 production. CO mixing ratios are in comparison especially high in the BL due to fresh urban pollution. The rapid uplift of these CO-rich BL airmasses in deep convection causes a second CO maximum in the UT ("C"-shape). During AMMA, the convective uplift of trace gases was most prominent between 12° N and 14° N, the region where large MCS pass by. Large amounts of NO_x, emitted from anthropogenic pollution and/or from soils in the Sahel zone by wetting from precipitation, may also reach the UT by transport within these MCS.

During convective uplift, the chemical composition in the UT is clearly influenced by the conditions in the BL and in addition by the BL height (Sect. 2.2). Within the framework of AMMA, observations by Crumeyrolle et al. (2011) show that elevated BL heights in the range of ∼1.5 km can

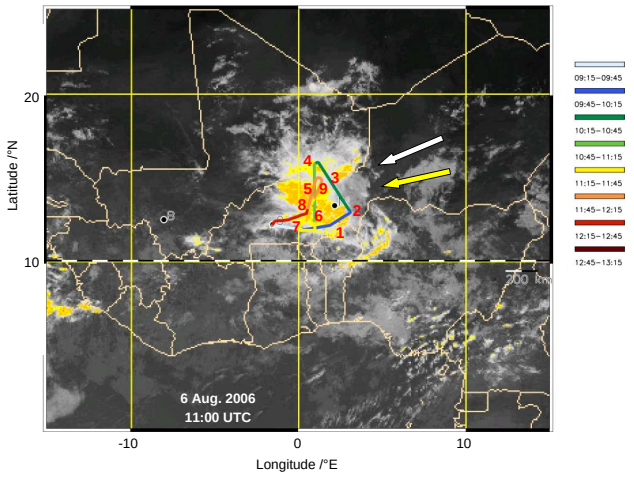

Fig. 2. Meteosat Second Generation (MSG) brightness temperatures over West Africa on 6 August 2006 at 11:00 UTC (orange 210 K, yellow 225 K). Superimposed are the Falcon flight track from Ouagadougou in Burkina Faso (colour-coded according to UTC time) and the sequences with elevated NO mixing ratios ($\geq$0.3 nmol mol^{-1}) labelled 1–9. Capital cities of Mali and Niger are indicated with black dots (B = Bamako to the west, N = Niamey to the east). The white arrow indicates the direction of the storm motion and the yellow arrow the main wind direction in the anvil outflow (not scaled according to velocity).

be present slightly north of 10° N along the meridian from Niamey to Cotonou. Towards the south, BL heights decrease with decreasing latitude, due to the increasing fraction of forest/shrub cover. South of 10° N, the top of the BL mainly varies between 1.0–1.2 km. These important differences in BL height will be discussed later in more detail.

3.2 Flight summary of 6 August 2006 and chemical composition

On 6 August 2006, an extended, circular MCS passed Niamey from northeast in the early morning hours and proceeded rapidly southwestward ($\sim$15 m s^{-1}). The Ouagadougou area was attained at noon. A series of MSG satellite images from 03:30–12:30 UTC indicates the temporal development of the convection before and during the mission flight (Fig. 1a–d). The Falcon flight track is superimposed in the satellite images. The aircraft started at 09:23 UTC in an easterly direction and first penetrated the southern part of the approaching MCS. Thereafter, the aircraft headed north along the rear side of the MCS and finally it investigated the area around the convective core with lightning. After passing Niamey at $\sim$08:30 UTC, the system was in a decaying stage and therefore easy to penetrate with the aircraft. Cloud tops reached up to $\sim$13 km and the large MCS expanded in a north-south direction over $\sim$500 km (12–17° N) and in an east-west direction over $\sim$300–400 km (around 0° E). The system as a whole was investigated by the aircraft during 3.5 h. The main flight level was 10.0–11.6 km, well located within the main anvil outflow region (see Sect. 4.3). For more detailed studies, single flight segments with enhanced NO mixing ratios compared to the background were selected. In these segments NO peak values exceeded 0.3 nmol mol^{-1}, indicative of sources from lightning and/or from the BL. On the whole, 9 such flight segments were found, as indicated in Fig. 2. Most of them were located at the edge of the MCS, however segment 5, 6, 8, and 9 were located closer to the convective core.

In Fig. 3a–c, time series of trace gas measurements (NO, NO_x, NO_y, HCHO, CO, O_3), and the wind velocity and direction are presented for the flight on 6 August. The Falcon ascent indicates that the AEJ was present in a layer between 3 and 5 km, with wind velocities from the east up to 11–13 m s^{-1} controlling the proceeding of the MCS (Fig. 3a). ECMWF wind analyses indicate that the AEJ core (max. 18 m s^{-1}) was located slightly north of the MCS, between 15–20° N and at pressure levels between 700 and 500 hPa (Fig. 4). Above 9 km ($\sim$300 hPa) and south of 10–15° N, a pronounced TEJ (max. 30 m s^{-1}) was present in the analyses. In agreement, elevated wind velocities from northeast in the range of 20–25 m s^{-1} were observed in the UT ($\sim$9.5–11.5 km) just ahead of the MCS (Figs. 3a and 5b), indicating the presence of a strong outflow downwind of the MCS. In contrast, on the rear (upwind) side of the MCS wind velocities were low $<$5 m s^{-1}, also mainly from the northeast. In this case, the prevailing easterly winds in the UT from the TEJ enhanced the outflow downwind of the MCS and reduced the outflow on the upwind side, where mixing with the ambient air already proceeded. According to ECMWF analyses, this typical monsoon MCS was located within the main region with strong updrafts (rainbelt of the ITCZ) located just north of the TEJ and south of the AEJ, as described in Sect. 3.1. The isothermes in Fig. 4 indicate that the height of the cold point tropopause was located at 16 km.

For an overview of the chemical conditions in the MCS outflow, the mean trace gas mixing ratios in the 9 selected flight segments from 6 August are listed in Table 2a, together with altitude, location and wind information. The distance to the convective core was estimated from MSG satellite images. The mean values of NO, NO_y and the NO/NO_y ratio were 0.27, 0.87 nmol mol^{-1} and 0.30, respectively, indicative of aged emissions. The mean CO, O_3, and HCHO mixing ratios were 102, 38, and 0.44 nmol mol^{-1}, respectively, indicative of airmass transport from the top of the BL, as discussed below. As discussed later in Sects. 4.2 and 5 in more detail, the main MCS inflow region (=top of the BL) was located rather high on this day, at $\sim$1.5 km altitude (see also Sect. 2.2).

The NO mixing ratios were only slightly enhanced by a few tenth of nmol mol^{-1} in the selected flight segments within the anvil outflow, compared to the background which already contained $\sim$0.1–0.2 nmol mol^{-1} NO (Fig. 3b). In all of the selected flight segments, rather similar mean NO

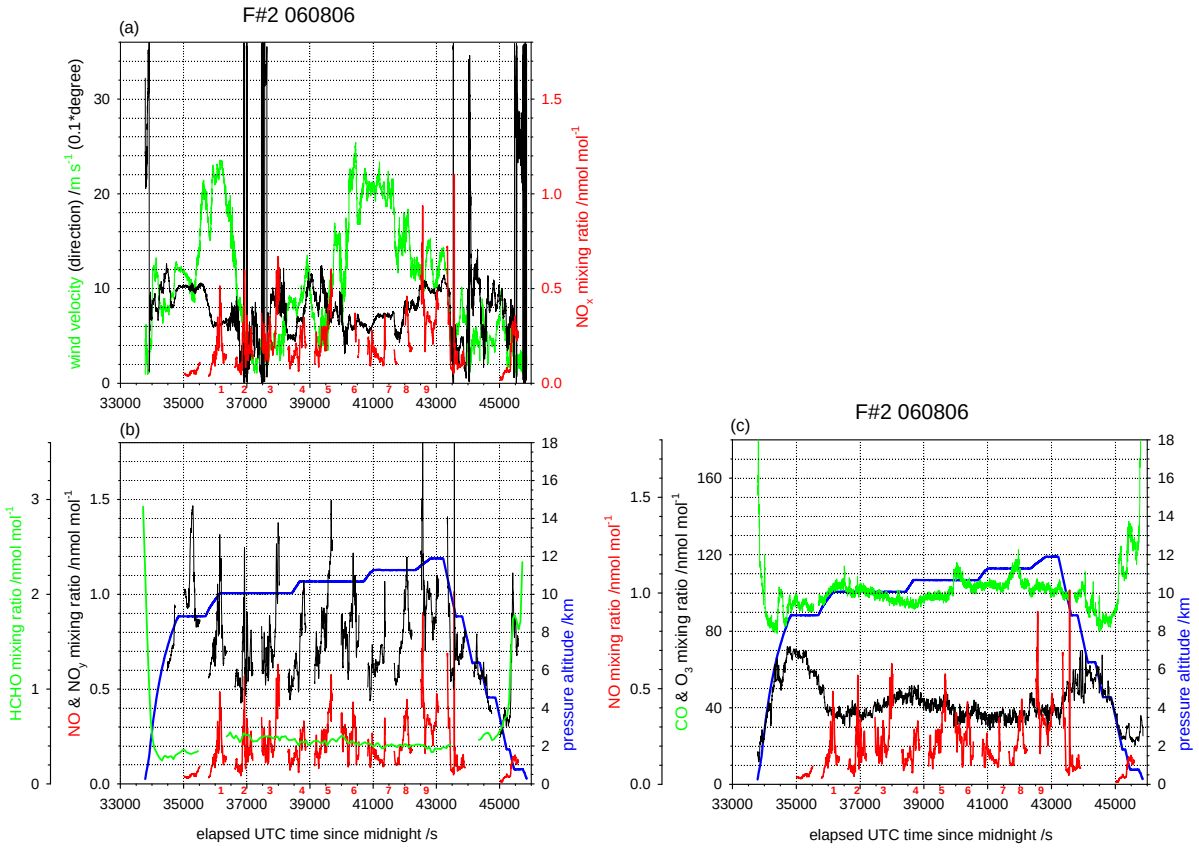

Fig. 3. Time series of NO_x, wind velocity and direction in **(a)**, NO, NO_y, HCHO, and pressure altitude in **(b)**, and NO, CO, O_3, and pressure altitude in **(c)** for the Falcon flight on 6 August 2006. Sequences with elevated NO mixing ratios ($\geq$0.3 nmol mol^{-1}) are labelled 1–9 in red.

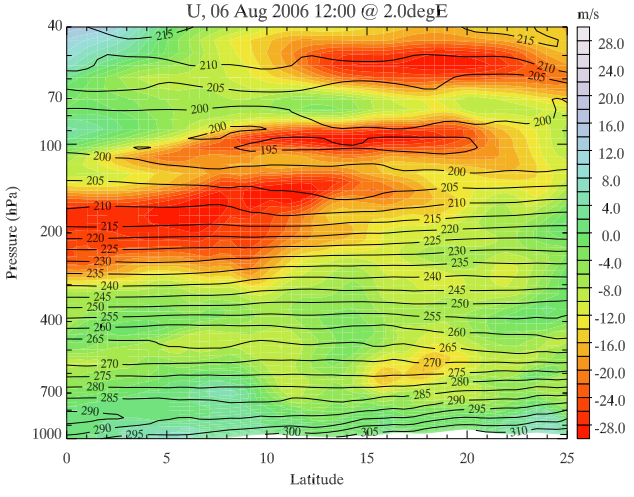

Fig. 4. ECMWF wind velocity and temperature (in K) analyses (vertical cross section for *u*-component) for 6 August 12:00 UTC along 2° E.

mixing ratios were observed (range 0.21–0.36 nmol mol^{-1}), with a tendency to higher values closer to the convective core. In flight segment 9, the highest mean NO mixing ratio (0.36 nmol mol^{-1}) and peak value (0.90 nmol mol^{-1}) were observed. This flight segment was located close to the convective core and it was the highest flight level (11.6 km) achieved within the MCS. The low ratios of NO to NO_y (0.26–0.36) found in the selected flight segments in general, indicate that a large fraction of NO was already aged and not produced by fresh lightning. Furthermore, a large fraction of the NO_x enhancement in the anvil outflow probably came from the BL, with NO_x mixing ratios at the top of the BL (here $\sim$1.5 km) in the range of $\sim$0.15–0.20 nmol mol^{-1}. In contrast, our results from the SCOUT-O3 campaign in Darwin in 2005 (Huntrieser et al., 2009) showed a strong contribution from LNO_x ($\geq$90%) and only a minor contribution from the BL to the high mean NO mixing ratios ($>$2 nmol mol^{-1}) observed in the outflow of a large MCS known as Hector. Furthermore, the high ratio of NO to NO_y ($\sim$0.7–0.8) found in Hector indicates that NO was emitted recently and most likely by lightning.

The HCHO mixing ratios during the flight on 6 August were rather constant in the vicinity of the MCS, varying

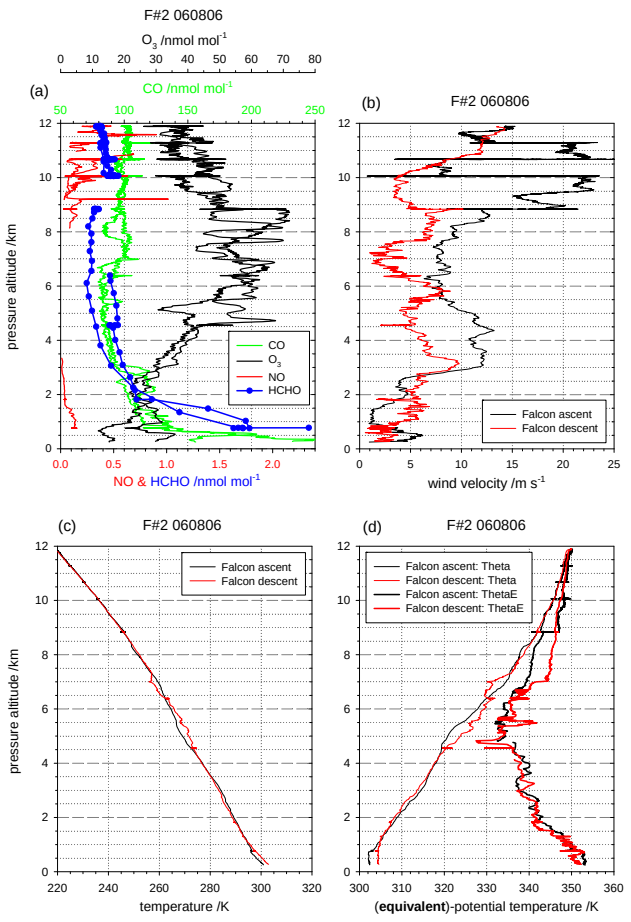

Fig. 5. Vertical profiles for CO, O_3, HCHO, and NO **(a)**, wind velocity **(b)**, temperature **(c)**, and (equivalent)-potential temperature **(d)** derived from Falcon measurements on 6 August 2006.

between ∼0.4 and 0.5 nmol mol^{-1}. The mixing ratios were rather independent of the distance to the convective core and only slightly higher as the range ∼0.3–0.4 nmol mol^{-1} observed in the ambient air (Fig. 3b). In contrast, mixing ratios were distinctly higher at the top of the BL, closer to the sources, and in the range of ∼1.0–1.5 nmol mol^{-1}. These observations of only slightly enhanced HCHO mixing ratios in the outflow also support the finding that the airmass transport from the BL to the UT was aged. HCHO is a very reactive trace gas with a short lifetime of a few hours. Scavenging within the cloud further contributes to reduce HCHO mixing ratios. Therefore, it is not expected to observe similar HCHO mixing ratios in the fresh MCS outflow as in the inflow region ("mirror" effect, Sect. 2.2).

The CO mixing ratios observed within the MCS outflow also show little variance (100 ± 5 nmol mol^{-1}) (Fig. 3c). Slightly higher mixing ratios (peak values up to 120 nmol mol^{-1}) were observed close to the convective core between the flight segments 5 and 6, and 7 and 8, indicative of direct transport from the MCS inflow region below, where also mixing ratios in the range of 110–130 nmol mol^{-1} were observed. In contrast, slightly lower mixing ratios (down to 90 nmol mol^{-1}) were observed at the rear side of the MCS between flight segments 3 and 4, which is close to ambient mixing ratios.

In comparison to the other trace gases with strong sources in the BL, the O_3 mixing ratios in the BL and within the MCS outflow were lower compared to the free troposphere ("S"-shaped vertical profile) and also showed little variance in the outflow region (∼40 nmol mol^{-1}) (Fig. 3c). In flight segments closer to the convective core, mean O_3 mixing ratios reached down to 35 nmol mol^{-1}. This value is however not as low as the mixing ratios observed at the top of the BL (∼25 nmol mol^{-1}), indicating that some mixing already took place in the outflow. This observation agrees well with recent finding by Avery et al. (2010) in the convective outflow of Central American thunderstorms during the TC4 campaign. In a simple calculation taking the O_3 production into account, their results indicate that mainly mixing with the ambient air and not O_3 production was responsible for the O_3 increase in the cloud outflow compared to the BL. Our AMMA-results for O_3 are rather different to our observations during SCOUT-O3, where a very efficient transport from the BL to the UT by deep convection was observed, actually "mirroring" the O_3-conditions in the BL (Huntrieser et al., 2009).

On the 6 August during AMMA, the highest O_3 mixing ratios were observed in the middle and upper troposphere outside of convection and just below the main outflow region. Within this ambient air, O_3 mixing ratios reached values between ∼60–70 nmol mol^{-1}), indicative of efficient O_3 production at these altitudes. This result is again very different to the rather low O_3 mixing ratios (∼40 nmol mol^{-1}) observed within the same altitude range over Brazil during TROCCINOX by Huntrieser et al. (2007) (=HH07), suggesting that West Africa has a much higher potential for O_3 production in the middle and upper troposphere.

Besides the flight from 6 August, many other Falcon flights focused on the trace gas composition in the monsoon MCS outflow (here only within ≤500 km distance selected). These flights on 1(b), 4, 7, 11, 15(a) and 18 August will only be discussed briefly (see Sect. 5), since rather similar behaviour and mixing ratios as on 6 August were observed. From all of these flights, about 30 flight segments were selected, on the same basis as described before. The mean values (±standard deviation) of NO, NO_y and the NO/NO_y ratio, carried out mainly in 10.3 ± 1.0 km altitude range, were 0.5 ± 0.2, 1.3 ± 0.5 nmol mol^{-1} and 0.35 ± 0.05, respectively, indicative of aged emissions with some contribution from lightning. The mean CO, O_3, and HCHO mixing ratios were 94 ± 7, 48 ± 5, and 0.46 ± 0.11 nmol mol^{-1}, respectively, indicative of aged airmass transport from the BL and subsequent mixing with the ambient air.

The trace gas and wind regime signatures described above are also clearly visible in the vertical profiles (see Fig. 5a–d).

Here also the temperature and equivalent-potential temperature profiles have been added to give additional information on the BL height. During the ascent, the monsoon layer with the southwesterly flow ($<6\,m\,s^{-1}$) reached up to $\sim$0.8 km altitude (Fig. 5b) and is also linked to an inversion layer (Fig. 5c and d). In the monsoon layer, the air was heavily polluted and CO mixing ratios exceeded $\sim$200 nmol mol^{-1}, whereas O_3 mixing ratios were very low (12–17 nmol mol^{-1}) due to efficient O_3 destruction mechanisms (Fig. 5a). Above the moist monsoon layer, a somewhat drier and cleaner transition layer followed which reached up to $\sim$1.4 km. Then between 1.4 and 1.5 km (=top of the BL) the wind changed abruptly to northeasterly-easterly directions (Fig. 3a) and the dry SAL is prominent. The range given for the top of the BL is in accordance with the range given for BL heights north of 10° N by Crumeyrolle et al. (2011), as discussed in Sect. 3.1. It seems that most of the air injected into the MCS originates from the bottom of the SAL at $\sim$1.5 km (see further more detailed discussions in Sects. 4.2 and 5), since the SAL acts as a barrier to the polluted layers below (Sect. 3.1). The temperature at the lifting condensation level was calculated according to Bolton (1980) from the mean temperature and humidity values for the lowest 100 m layer (see also Huntrieser et al., 2007). The mean temperature (301 K) and relative humidity (66%) in this layer from the Falcon ascent and descent resulted in a lifting condensation level temperature of 292.5 K corresponding to a cloud base height of 1.4–1.5 km. Since also emissions from lightning were not very prominent in this case, the NO/NO_y ratio was rather low indicating mainly aged emission transported from the top of the BL. The vertical profiles will be discussed in more detail in Sect. 4.

3.3 Flight summary of 15 August 2006 and chemical composition

On 15 August 2006, two flights were performed with the Falcon aircraft, however only the second one is discussed here in more detail (see Sect. 2.2). During this afternoon flight, a smaller MCS moving rapidly ($\sim$18 m s^{-1}) from Benin to Togo was investigated in detail (Fig. 6). The system originated from a huge, circular MCS that passed over Northern Nigeria ($\sim$11–14° N) already at midnight. Until 06:00 UTC this system moved southwestward and almost dissipated. At 07:00 UTC, a new growing cell developed out of the remnants of this system and passed the border to Benin at 09:00–10:00 UTC. This smaller MCS then proceeded south of 10° N, further equatorward than all other MCS investigated by the Falcon aircraft. In this region more vegetation is present, due to the vicinity to the equatorial, tropical rain forest. The dimension of the MCS in north-south direction was $\sim$150–250 km, in east-west direction $\sim$50–100 km (around 0° E) and cloud tops reached up to $\sim$13 km. The main flight level was 10.1–11.9 km, again well located within the main anvil outflow region (see Sect. 4.3).

The aircraft started at 14:37 UTC in a southeasterly direction and first penetrated the northern edge of the MCS outflow. Thereafter, the aircraft headed south along the rear side of the MCS, approached the convective core from the back, performed some turns, and finally returned to Ouagadougou after a short 2.5 h flight. For more detailed studies, single flight segments with enhanced NO mixing ratios compared to the background were selected, as described in the previous case. On the whole, 7 such flight segments were found, as indicated in Fig. 6. Most of them were located at the edge of the MCS, however segment 3, 4, and 5 were located close to the convective core.

In Fig. 7a–c, time series of trace gas measurements (NO, NO_x, NO_y, HCHO, CO, O_3), and the wind velocity and direction are presented for the flight on 15 August. The Falcon ascent from Ouagadougou indicates that the AEJ was somewhat more elevated on this day characterised by a mean wind velocity of 15 m s^{-1} in the layer between 3 and 6 km. The AEJ was especially pronounced at $\sim$4.5 km altitude, with wind velocities from the east to northeast reaching up to 24 m s^{-1} (Fig. 7a). ECMWF wind analyses indicate that a strong AEJ core (max. 24 m s^{-1}) was located slightly north of the MCS, between 10–15° N and at pressure levels between 700 and 450 hPa (Fig. 8). Above 9 km ($\sim$300 hPa) and between 5–10° N, no pronounced TEJ was present in the analyses, as in the previous case. In accordance, wind velocities in the UT within the investigated MCS over Benin and Togo were in general lower compared to the first investigated case from 6 August. The highest wind velocities ($\sim$16 m s^{-1}) were measured directly at the rear side of the MCS from easterly to southeasterly directions. The ambient air of the MCS came from the same direction, however the wind velocities were much lower and even reached down to $\sim$5 m s^{-1}. There are no indications of a nearby jet stream in the UT in accordance with the decreasing monsoon activity after mid August (see Sect. 3.1). The isothermes in Fig. 8 indicate that the height of the cold point tropopause was located at 15.5–16 km.

For an overview of the chemical conditions in the MCS outflow, the mean trace gas mixing ratios in the 7 selected flight segments from 15 August are listed in Table 2b, together with altitude, location and wind information. Overall, the trace gas values were slightly higher compared to the previous case discussed, indicative of stronger pollution transport from the BL. The mean values of NO, NO_y and the NO/NO_y ratio were 0.32, 1.03 nmol mol^{-1} and 0.32, respectively, indicative of aged emissions. The mean CO, O_3, and HCHO mixing ratios were 125, 47, and 0.60 nmol mol^{-1}, respectively, indicative of airmass transport from the BL, as discussed below and in Sects. 4.2 and 5 in more detail. Unfortunately, from this flight no information on the trace gas composition in the BL directly below and ahead of the investigated MCS was available. However, from other AMMA flights conducted by the BAe-146, it is known that BL mixing ratios in this region (9–10° N) were in the range of

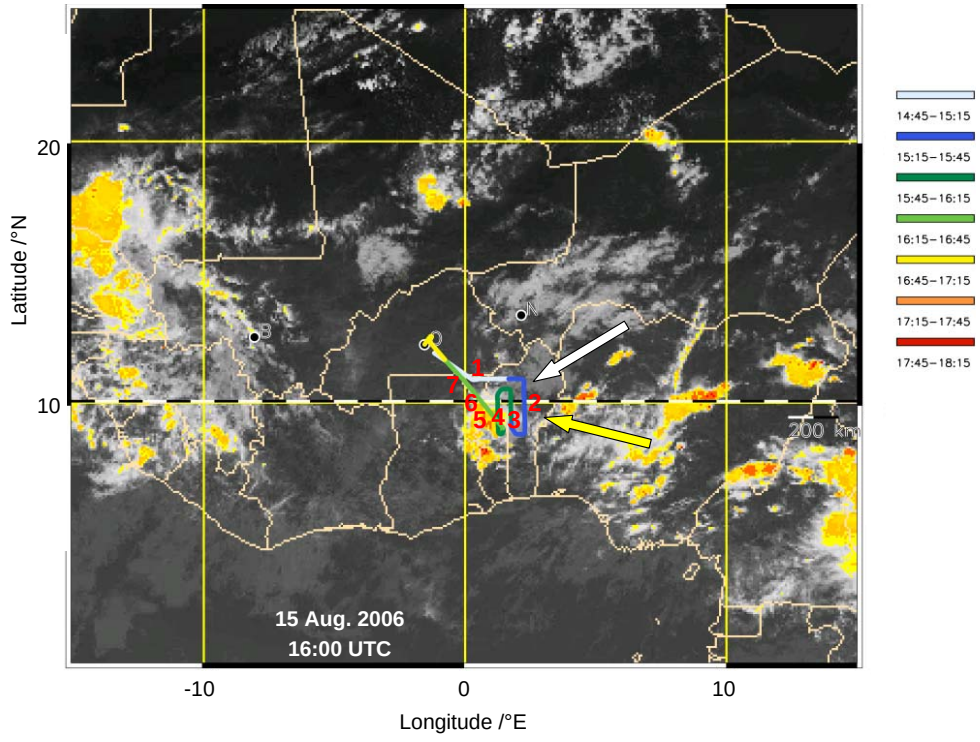

Fig. 6. Meteosat Second Generation (MSG) brightness temperatures over West Africa on 15 August 2006 at 16:00 UTC (red 195 K, orange 210 K, yellow 225 K). Superimposed are the Falcon flight track from Ouagadougou in Burkina Faso (colour-coded according to UTC time) and the sequences with elevated NO mixing ratios ($\geq$0.3 nmol mol^{-1}) labelled 1–7. Capital cities of Mali and Niger are indicated with black dots (B = Bamako to the west, N = Niamey to the east). The white arrow indicates the direction of the storm motion and the yellow arrow the main wind direction in the anvil outflow (not scaled according to velocity).

$\sim$120–160 nmol mol^{-1} for CO, $\sim$20–30 nmol mol^{-1} for O_3, and $\sim$0.8–1.2 nmol mol^{-1} for HCHO (Reeves et al., 2010).

In all of the selected flight segments (Fig. 7b), rather similar mean NO mixing ratios were observed (range 0.22–0.47 nmol mol^{-1}), as in the previous case. Within the MCS, a tendency to increasing NO mixing ratios with altitude was observed (segment 3 to 6). In flight segment 6, the highest mean NO mixing ratio (0.47 nmol mol^{-1}) and peak value (1.09 nmol mol^{-1}) were observed. This flight segment was located at the northern edge of the convective core and it was again the highest flight level (11.7 km) achieved within the MCS. The low ratios of NO to NO_y (0.15–0.40) found in the selected flight segments in general, indicate that a large fraction of NO was already aged and not produced by lightning. The increasing NO/NO_y ratios with altitude within the MCS (and the constant CO mixing ratios) indicate that the contribution from lightning to the total NO (and NO_x) content increased with altitude (Table 2b). However, a large contribution to the NO_x enhancement in the anvil outflow probably came from the BL (see further discussion in Sects. 4.2 and 5).

The HCHO mixing ratios during the flight on 15 August were slightly enhanced ($\sim$0.6–0.7 nmol mol^{-1}) during the penetrations of the flight segments 3, 4, and 5 located close to the convective core, indicative of direct upward transport from the BL (Fig. 7b). However, within these three flight segments, the mean HCHO mixing ratios decreased with altitude whereas the mean CO mixing ratios remained constant. HCHO seems to be a less useful tracer for BL air as CO, due to its much shorter lifetime and higher reactivity. Scavenging within the cloud further contributes to reduce HCHO mixing ratios. In addition, HCHO mixing ratios clearly decreased with increasing distance from the convective core. In the ambient air, HCHO mixing ratios were in the range of $\sim$0.4–0.5 nmol mol^{-1} and slightly higher as in the previous case. The reasons for the higher HCHO mixing ratios in general during this flight, can be explained by the different conditions in the BL. More vegetation and forest is present south of 10° N that emits higher amounts of hydrocarbons like isoprene (Bechara et al., 2010; Reeves et al., 2010). Large amounts of HCHO can be produced by photooxidation of these biogenic isoprene emissions (Dufour et al., 2009). Biomass burning, another source of HCHO, is also more relevant at these latitudes (Real et al., 2010). Barret et al. (2008) observed a maximum in the upper tropospheric CO mixing ratios around 5° N during the monsoon season, which they attributed to elevated biomass burning plumes. Furthermore, the BL air in the MCS outflow was probably uplifted from lower altitudes (no capping SAL over

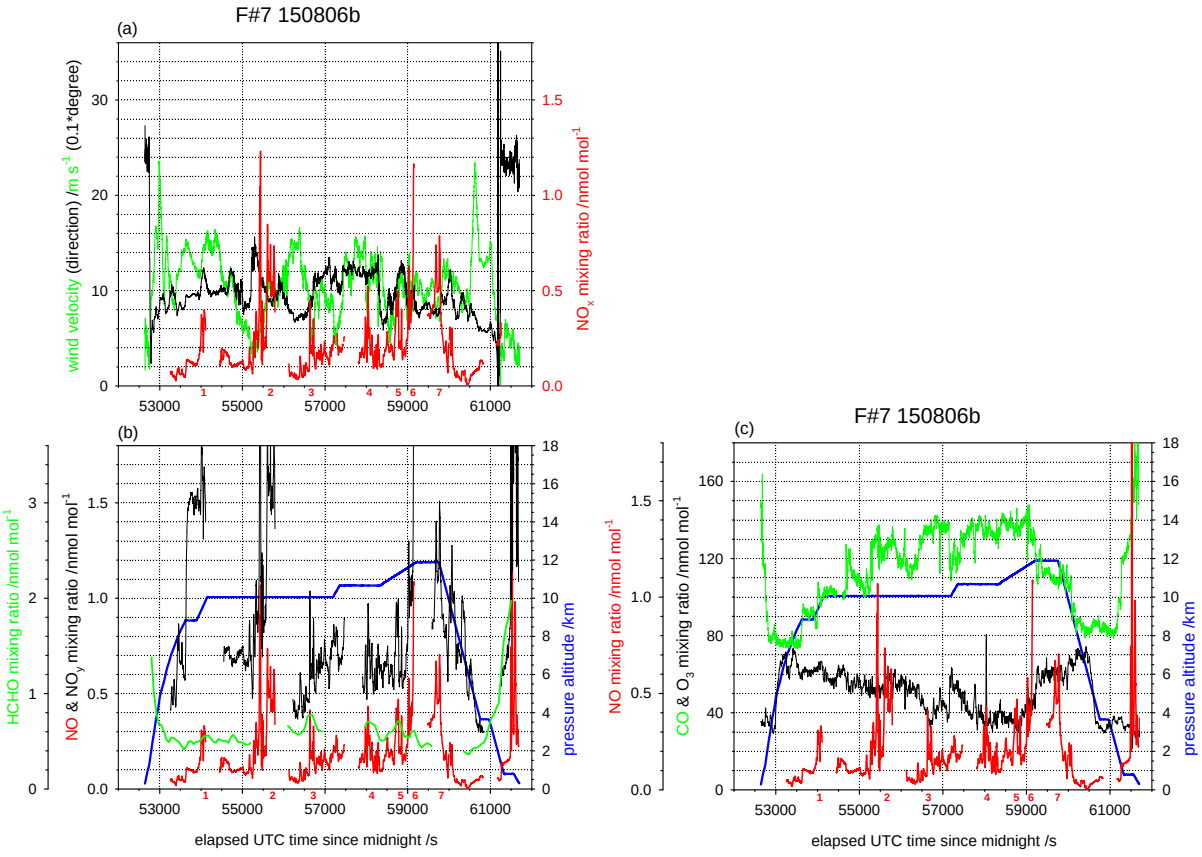

Fig. 7. Time series of NO_x, wind velocity and direction in **(a)**, NO, NO_y, HCHO, and pressure altitude in **(b)**, and NO, CO, O_3, and pressure altitude in **(c)** for the Falcon flight on 15 August 2006. Sequences with elevated NO mixing ratios ($\geq$0.3 nmol mol^{-1}) are labelled 1–7 in red.

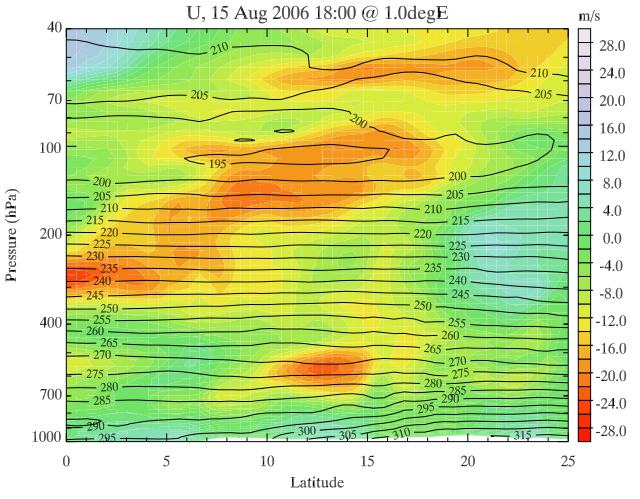

Fig. 8. ECMWF wind velocity and temperature (in K) analyses (vertical cross section for u-component) for 15 August 18:00 UTC along 1° E.

Benin-Togo) compared to the previous case and therefore it was more strongly polluted (see below).

The CO mixing ratios observed within the MCS outflow on 15 August were distinctly enhanced, indicative of a larger amount of fresh emissions transported from the BL, compared to the previous case (Fig. 7c), see also detailed discussions in Sect. 5. The highest mean mixing ratios were observed close to the convective core ($\sim$135 nmol mol^{-1}), whereas mixing ratios clearly decreased with increasing distance from the convective core. At a distance of 100–150 km from the core in northerly directions, the CO mixing ratios were close to ambient mixing ratios observed north of 10° N.

In comparison to the previous case from 6 August, with only slightly changing O_3 mixing ratios in the anvil outflow region, the O_3 mixing ratios on 15 August showed a much stronger tendency to increasing values with increasing distance from the convective core (Fig. 7c, Table 2b). In flight segments close to the convective core, mean O_3 mixing ratios reached down to 34 nmol mol^{-1}, which is however similar as in the previous case. During take-off and landing in Ouagadougou on 15 August, O_3 and CO mixing ratios within a similar range ($\sim$30–35 and $\sim$120–160 nmol mol^{-1},

respectively) were observed at the top of the BL, as in the fresh MCS outflow. In this case it is not known how representative these BL conditions are for the actual conditions in the MCS inflow region south of 10° N over Benin-Togo, however these values agree rather well with the mixing ratios observed by the BAe-146 in the BL below 900 hPa, as given previously in this section (Reeves et al., 2010).

Within the three flight segments close to the convective core, rather constant CO and O_3 mean mixing ratios were observed, 134–135 and 34–38 nmol mol^{-1}, respectively, even as the aircraft stepwise climbed from 10.1 to 11.3 km. These observations are indicative of a rather undiluted transport of trace gases from the top of the BL in these flight segments. At the northern edge of the MCS (flight segment 6), the mean CO mixing ratio in the outflow was still unchanged with 136 nmol mol^{-1}, however the mean O_3 mixing ratio suddenly increased to 45 nmol mol^{-1}. Rapid mixing with the ambient CO- and O_3-rich air (impacted by aged biomass burning plumes) probably caused this rapid O_3 increase. About ∼50–100 km further upwind in flight segment 2, the mean O_3 mixing ratio even increased to 55 nmol mol^{-1}. On the other hand, the mean CO mixing ratio slightly decreased down to 126 nmol mol^{-1}, indicating further mixing with the ambient air. Further away from the convective core, about 100–150 km to the north, mixing with the ambient air continued in flight segments 1 and 7 and the mean mixing ratios of O_3 increased to 64 nmol mol^{-1} and of CO decreased to 96 nmol mol^{-1}. At this stage, the outflow mixed with the ambient air located north of 10° N, which contained less CO compared to further south (influenced by biomass burning plumes). According to the velocity in the MCS outflow, it takes at least 2–3 h for the MCS-processed airmass to reach this region. At this point, the airmass was already well mixed, and O_3 and CO mixing ratios reached ambient conditions in the UT north of 10° N, which were in the range of 60–70 and 80–100 nmol mol^{-1}, respectively.

The trace gas and wind regime signatures described above are also clearly visible in the vertical profiles (see Fig. 9a–d). In addition, the temperature and equivalent-potential temperature profiles have been added that give information on the BL height. During the ascent close to Ouagadougou, the monsoon layer with the southwesterly flow (<7 m s^{-1}) reached up to ∼1.2 km altitude (Fig. 9b) and was also linked to an inversion layer (Fig. 9c–d), as in the previous case. In the monsoon layer, the air was heavily polluted and CO mixing ratios exceeded ∼200 nmol mol^{-1}, whereas O_3 mixing ratios were rather low (30–35 nmol mol^{-1}), due to efficient O_3 destruction mechanisms (Fig. 9a). Above the moist monsoon layer, a somewhat drier and cleaner transition layer followed which reached up to ∼1.9 km. Above 2.0 km the wind changed to northeasterly-easterly directions and the dry SAL is prominent. It seems that most of the air injected into the MCS over Benin-Togo originated directly from the heavily polluted monsoon layer, since the SAL is less prominent south of 10° N. We assume, based on the measurements carried out close to Ouagadougou and from O_3/CO correlations discussed in Sect. 5, that the top of the BL in the Benin-Togo area was located between ∼0.8–1.2 km (Fig. 9a–d). This range is in accordance with the range given for BL heights south of 10° N by Crumeyrolle et al. (2011), as discussed in Sect. 3.1. The higher amount of O_3 precursors in the MCS outflow on 15 August, may promote the production of O_3 in a later stage. This important issue will be discussed in more detail in Sect. 5.

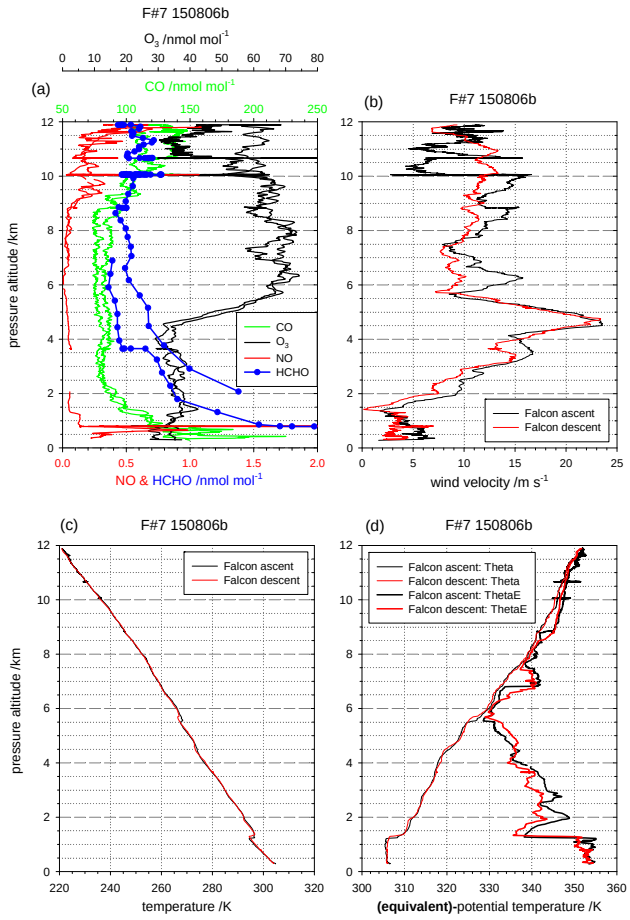

Fig. 9. Vertical profiles for CO, O_3, HCHO, and NO **(a)**, wind velocity **(b)**, temperature **(c)**, and (equivalent)-potential temperature **(d)** derived from Falcon measurements on 15 August 2006.

3.4 Spatial and temporal LINET stroke distributions

3.4.1 Case 6 August 2006

On 6 August 2006, the extended monsoon MCS between Ouagadougou and Niamey was located along the northern periphery of the LINET lightning location network, however just within the range of coverage for stroke detection. Unfortunately, the power supply of the LINET sensors was out of order in the morning of the 6 August. After 11:03 UTC,

Table 2. Trace gas measurements in the anvil outflow of the MCS investigated on 6 and 15 August 2006.

Flight, anvil penetration and field experiment	Entry and exit time (UTC), s	Pressure altitude, km	Distance from deep convective region, km	Wind direction	Mean anvil NO mixing ratio, nmol mol^{-1}	Mean anvil NO_y mixing ratio, nmol mol^{-1}	NO/NO_y	Mean anvil CO mixing ratio, nmol mol^{-1}	Mean anvil O_3 mixing ratio, nmol mol^{-1}	Mean anvil HCHO mixing ratio, nmol mol^{-1}
(a)										
060806a_P1 AMMA	36 041–36 246	10.0	edge MCS	NE	0.26	0.94	0.27	103	37	–
060806a_P2	36 853–37 157	10.1	edge MCS	NE	0.23	0.72	0.31	102	36	0.50
060806a_P3	(<)37 468-(>)38 030	10.1	edge MCS	E	0.26	0.78	0.31	98	42	0.49
060806a_P4	38 669-(>)38 870	10.7	edge MCS	NE-E	0.24	0.89	0.27	94	47	0.45
060806a_P5	39 359–40 198	10.7	inside MCS	NE-E	0.30	0.91	0.32	102	39	0.47
060806a_P6	40 236–40 465	10.7	inside MCS	NE	0.28	0.94	0.29	105	36	0.45
060806a_P7	41 351–41 687	11.3	edge MCS	NE	0.21	0.79	0.26	104	35	0.41
060806a_P8	41 822–42 230	11.3	inside MCS	NE	0.25	0.86	0.28	109	35	0.41
060806a_P9	(<)42 508–43 452	11.6	inside MCS	E	0.36	0.99	0.36	102	39	0.38
mean					**0.27**	**0.87**	**0.30**	**102**	**38**	**0.44**
(b)										
150806b_P1 AMMA	53 945-(>)54 111	9.5	100–150	E-SE	0.23	1.58	0.15	96	64	0.54
150806b_P2	55 260-(>)55 786	10.1	50–100	E-SE	0.37	1.26	0.28	126	55	–
150806b_P3	56 620–56 740	10.1	inside MCS	E	0.22	0.69	0.31	135	36	0.73
150806b_P4	57 959–58 094	10.7	inside MCS	E-SE	0.26	0.70	0.36	134	38	0.67
150806b_P5	58 671–58 871	11.3	inside MCS	E-SE	0.29	0.74	0.38	135	34	0.64
150806b_P6	58 998-(>)59 149	11.7	edge MCS	E	0.47	1.15	0.40	136	45	0.58
150806b_P7	(<)59 487–59 877	11.7	∼100	E	0.40	1.07	0.38	110	60	0.47
mean					**0.32**	**1.03**	**0.32**	**125**	**47**	**0.60**

the system was operating normally again. At this time the aircraft just entered flight segment 5 close to the convective core. The spatial distribution of all LINET strokes with peak currents ≥1 kA between 11:03 and 15:00 UTC (black dots) is shown in Fig. 10a together with the Falcon flight track and measured NO mixing ratios (coloured). The selected flight segments are labelled as before. Since the MCS was located far away from the LINET sensors, as indicated in Fig. 10a, the detection efficiency of the network for low peak currents was reduced and only strokes with peak currents above 5 kA were registered within the MCS (superimposed as coloured dots). From Fig. 10a it is obvious that the strokes originated along a line perpendicular to the wind direction from northeast. This type of organised systems is known as squall line mesoscale convective systems (SLMCS) (Rickenbach et al., 2009). The confluence of the monsoon layer and SAL, and the resulting AEJ provides the necessary low level shear for the initiation and maintenance of these squall lines (Rowell and Milford, 1993). Figure 10a also indicates that the highest frequency of elevated NO mixing ratios along the flight track is observed close to the convective core with lightning and directly behind it. The temporal evolution of the strokes, indicated within the SLMCS in colour, shows a rather slow movement southwestward (6–7 m s^{-1}) since the system was in a decaying stage.

A time series of LINET stroke rates for this case is presented in Fig. 11a. For an adequate comparison of the stroke rates in different storms, it was necessary to restrict comparisons to higher stroke peak currents (≥10 kA). These were observed with about the same detection efficiency, independent of their location within the LINET network, as discussed in HH08 and in Huntrieser et al. (2009) (=HH09). The SLMCS of 6 August was mainly in a lightning decaying stage during the aircraft passage and stroke rates were low but rather constant. The highest stroke rates within the SLMCS were observed around 11:25–11:30 UTC (between flight segment 6 and 7) and around 12:40–12:45 UTC with 24 strokes (≥10 kA) per 5 min in both cases. This value is very low compared to our previous observations in other tropical regions. For comparison, the highest stroke rates observed during TROCCINOX in a subtropical and in tropical thunderstorms (HH08) were ∼80 and 40 strokes per 5 min, respectively. During SCOUT-O3, even stroke rates up to almost 400 strokes per 5 min were observed in Hector (HH09).

3.4.2 Case 15 August 2006

On 15 August 2006, the MCS between Benin and Togo was located within the centre of the LINET lightning location network with the highest detection efficiency. The spatial distribution of all LINET strokes with peak currents ≥1 kA between 11:00 and 18:00 UTC (black and coloured dots) is shown in Fig. 10b together with the Falcon flight track and measured NO mixing ratios (coloured). The selected flight segments are labelled as before.

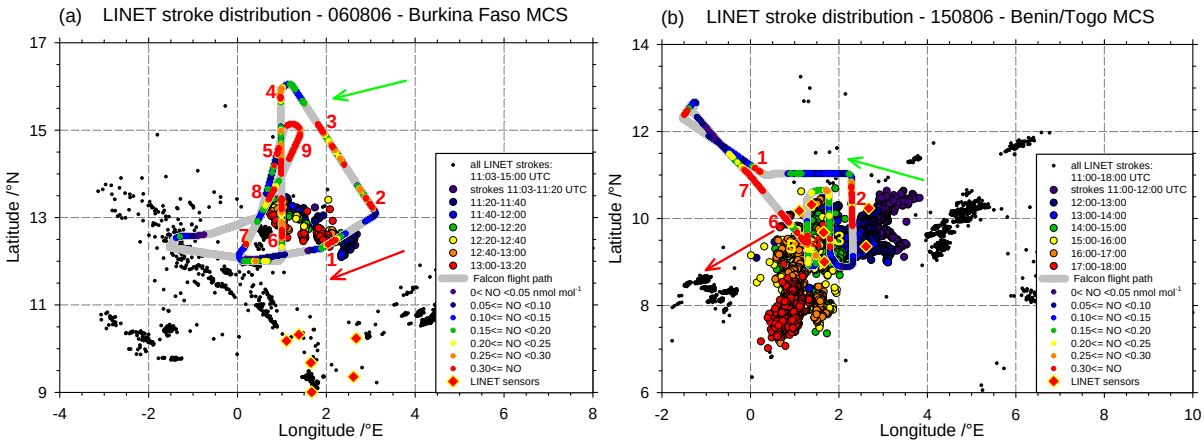

Fig. 10. Spatial and temporal LINET stroke distribution on 6 August 2006 at 11:03–15:00 UTC **(a)** and on 15 August 2006 at 11:00–18:00 UTC **(b)** (upper colour scale: only selected thunderstorm system). On 6 August, LINET data were not available before 11:03 UTC. The observed NO mixing ratio along the Falcon flight path is superimposed (lower colour scale). Sequences with enhanced NO mixing ratios were observed within the MCS outflow (labelled in red). The red arrow indicates the direction of the storm motion and the green arrow the main wind direction in the anvil outflow (not scaled according to velocity). In addition, the positions of the LINET sensors are indicated (diamonds).

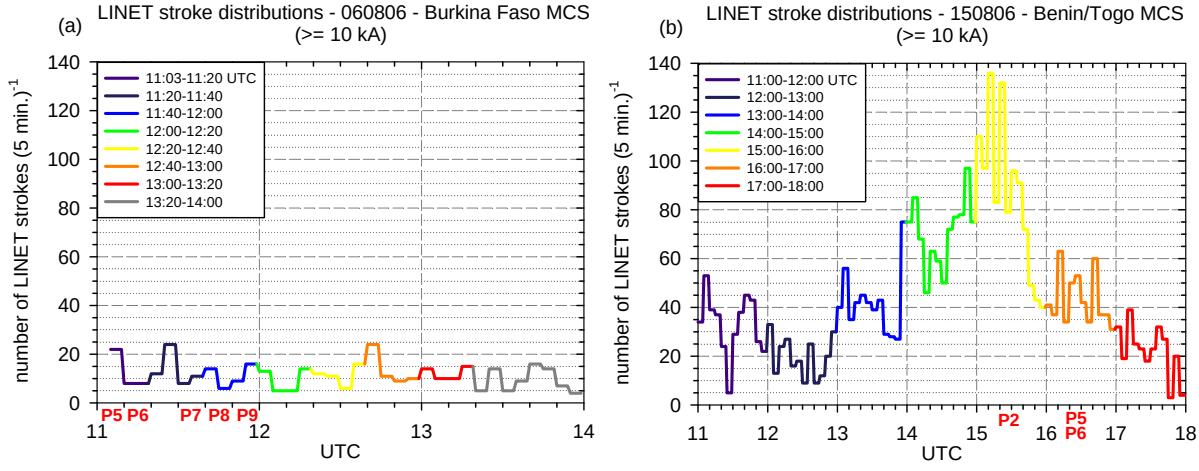

Fig. 11. Time series of LINET stroke rates (colour-coded as in Fig. 10) determined for the selected thunderstorm systems on 6 August **(a)** and 15 August 2006 **(b)** (only strokes with peak currents ≥10 kA considered). The times when the different anvil penetrations took place are labelled in red below the time scale.

From Fig. 10b it is obvious that the strokes developed less structure compared to the previous case and also merging of single cells took place. The movement of the MCS and the wind direction in the anvil outflow region are indicated with arrows. In this case the system moved rather rapidly southwestward (12–13 m s^{-1}), however the outflow was advected rather slowly to the northwest since no jet stream was present in this area. Figure 10b also indicates that the highest frequency of elevated NO mixing ratios along the flight track were observed along the northern edge of the MCS, just downwind of the system.

A time series of LINET stroke rates for this case is presented in Fig. 11b. As the aircraft approached the MCS, it was in a mature stage and thereafter the stroke rate decreased. The highest stroke rates within the MCS were observed around 15:10–15:15 UTC with 136 strokes (≥10 kA) per 5 min, just before the penetration of flight segment 2 at the rear side of the MCS. This value is slightly higher than observed in the investigated thunderstorms during TROCCINOX (HH08), however still distinctly lower compared to observations in Hector during SCOUT-O3 (HH09).

4 Estimate of the LNO_x production rate per flash and per year

In this section, the measurements in the selected MCS of 6 and 15 August 2006 are discussed in more detail and the resulting annual global nitrogen mass production rate by lightning is determined. The values needed for the calculations are estimated according to the equations below.

First the method used to estimate the annual global LNO_x nitrogen mass production rate G_{LNO_x} (in $Tg\,a^{-1}$) is briefly introduced. The same method was already applied in HH08 and HH09. For an overview of the different steps, see Fig. 3 in HH08. More details are also given later in Sect. 4. The method is based on the idea that most LNO_x produced in a thunderstorm is transported into the anvil region, as indicated in many recent studies based on cloud-model simulations (e.g., Ott et al., 2010).

The horizontal LNO_x mass flux F_{LNO_x} (in nitrogen mass per time, $g\,s^{-1}$) is calculated from measurements during each anvil penetration according to Chameides et al. (1987):

$$F_{LNO_x} = \chi_{LNO_x} \cdot \frac{M_N}{M_{air}} \cdot \rho_a (V_a - V_s) \cdot \Delta x \cdot \Delta z \quad (1)$$

where χ_{LNO_x} is the mean NO_x volume mixing ratio produced by lightning ($mol\,mol^{-1}$), M_N and M_{air} are the molar masses of nitrogen ($14\,g\,mol^{-1}$) and air ($29\,g\,mol^{-1}$), respectively, ρ_a is the air density ($g\,m^{-3}$) calculated from measured temperature and pressure in the anvil, and $V_a - V_s$ is the difference between the wind vectors in the anvil outflow and at the steering level. In general, the wind at the steering level ($\sim$700 hPa) determines the mean motion of a thunderstorm cell (Keenan and Carbone, 1992). However, this parameter was not available from every flight since this region was not probed specifically. The storm motion (V_s) was instead determined from the spatial LINET stroke evolution based on horizontal stroke distributions with a high temporal resolution of 10 min. The last term $\Delta x \cdot \Delta z$ is the area (m^2) of the vertical cross-section perpendicular to the wind direction in the anvil outflow. The parameters in Eq. (1), except Δx and Δz, were calculated directly from Falcon measurements by averaging the measured data over the time period when the anvil was penetrated.

For the estimate of the LNO_x production rate P_{LNO_x} (nitrogen mass per stroke, in g $stroke^{-1}$) in a thunderstorm, the horizontal LNO_x mass flux F_{LNO_x} ($g\,s^{-1}$) is then divided by the total (IC+CG) contributing LINET stroke rate R_{LINET} ($strokes\,s^{-1}$) according to HH08:

$$P_{LNO_x} = \frac{F_{LNO_x}}{R_{LINET}} \quad (2)$$

For comparison with other published results, the P_{LNO_x} estimates per LINET stroke in Eq. (2) are scaled to P_{LNO_x} estimates per LIS flash. Finally, it is multiplied with the number of LIS flashes occurring globally, 44 ± 5 $flashes\,s^{-1}$ according to Christian and Petersen (2005), to achieve the annual global LNO_x nitrogen mass production rate G_{LNO_x} (in $Tg\,a^{-1}$).

This section is organised in the following subsections: The spatial and temporal distributions of LINET strokes presented in Sect. 3.4 are used in Sect. 4.1 to associate the individual anvil-NO_x enhancements to corresponding LINET strokes and representative stroke frequencies. The contribution of BL-NO_x and LNO_x to measured anvil-NO_x is estimated in Sect. 4.2. For the calculation of the horizontal LNO_x mass flux rate, the mean depth of the anvil outflow is estimated in Sect. 4.3. The horizontal LNO_x mass flux rate out of the anvils is calculated by means of estimated LNO_x mixing ratios and horizontal outflow wind velocities from the flights combined with the size of the vertical cross-section of the anvils (Sect. 4.4). LNO_x nitrogen mass flux rates ($g\,s^{-1}$) and LINET stroke rates ($strokes\,s^{-1}$) are then combined to estimate the production rate of LNO_x (in g of nitrogen mass or number of NO_x molecules) per LINET stroke and per LIS flash (Sect. 4.5). Finally, the annual global LNO_x nitrogen mass production rate G_{LNO_x} in $Tg\,a^{-1}$ is estimated.

4.1 Contribution from observed LINET strokes to measured anvil-NO_x and resulting stroke rates

For the estimate of the LNO_x production rate per stroke, it is important to know which of the registered LINET strokes contributed to the estimated LNO_x enhancement in the anvil outflow. Presently, cloud-scale modelling is most suitable for this task (e.g., Ott et al., 2007). For several TROCCINOX, SCOUT-O3/ACTIVE and AMMA cases cloud-resolving model simulations are in preparation, but not ready yet (Huntemann et al., 2011; K. Pickering, NASA Goddard, personal communication, 2010). Here we use a rough approximation to estimate the number of LINET strokes contributing to LNO_x. Comparisons between this method of advecting strokes with the ambient wind measured by the aircraft and lightning tracer simulations with a Lagrangian particle dispersion model (FLEXPART) in HH08 indicated that this method alternatively can be used. It is known from cloud-model simulations that most LNO_x produced in a thunderstorm is transported into the anvil region (Skamarock et al., 2003; Fehr et al., 2004; Ott et al., 2010).

On 6 August, the power supply of the LINET network was out of order in the morning and started to operate normally again after 11:03 UTC. At this time the aircraft already started to investigate the SLMCS and stayed within this system until 12:00 UTC. Within this given time period and area, the total number of strokes with peak currents $\geq$10 kA was 139, which gives a total stroke rate of 0.041 $strokes\,s^{-1}$. In this case, we assume that all of these strokes contributed to the measured anvil-NO_x in the flight segments along the SLMCS perpendicular to the wind direction (flight segments 4 to 6 and 7 to 9).

The first selected penetration from this case in Table 3 (P5-6) lasted from 10:56–11:14 UTC. For further calculations

Table 3. Estimates of horizontal LNO_x mass flux F_{LNO_x}, LINET stroke rate R_{LINET}, LNO_x production rate per LINET stroke and per LIS flash P_{LNO_x}, and global LNO_x production rate per year G_{LNO_x} for selected AMMA thunderstorm penetrations.

Flight, flight segment and field experiment	Entry and exit time (UTC), s	Latitude (° N)/ longitude (° E)	Pressure altitude, km	Mean $\chi^1_{BL\text{-}NO_x}$, nmol mol^{-1}	Mean $\chi^2_{LNO_x}$, nmol mol^{-1}	$\lvert V_a - V_s\rvert^3$, m s^{-1}	ρ_a, kg m^{-3}	Δx, km	Δz, km	$F^4_{LNO_x}$, g(N) s^{-1}	R^5_{LINET}, (LINET strokes) s^{-1}	$P^6_{LNO_x}$, g(N) (LINET stroke)$^{-1}$	$P^7_{LNO_x}$, g(N) (LIS flash)$^{-1}$	G_{LNO_x}, Tg(N) a^{-1}
060806_P5-6 (SLMCS) AMMA	39 359–40 458	+13 to 15/along+1	10.7	0.16 (48%)	0.17	6.6	0.36	~220	~3	129	0.041	3139	2417	3.4
060806_P8–9 (SLMCS) AMMA	42 019–43 452	+13 to 15/along+1	11.5 (10.1–11.9)	0.16 (46%)	0.19	7.0	0.33	~220	~3	140	0.041	3411	2626	3.6
150806b_P5–6 (MCS) AMMA	58 671–59 149	+9 to 10/along+1	11.5 (11.1–11.8)	0.18 (53%)	0.16	8.9	0.33	~150	~2.5	85	0.066	1289	993	1.4
	relative max. error				~40%	~50%		~50%	~40%	~180%	~60%	~240%	~290%	300%

[1] Mean NO_x mixing ratio transported from the boundary layer (BL-NO_x) into the anvil outflow.
[2] Mean NO_x mixing ratio produced by lightning (LNO_x) in the anvil outflow (difference between total measured anvil-NO_x and the BL-NO_x contribution).
[3] True horizontal anvil outflow velocity (difference between the wind vectors in the anvil outflow and at the steering level). See Appendix.
[4] The horizontal LNO_x mass flux out of the anvil, see Eq. (1).
[5] Only LINET strokes with peak currents $\geq$10 kA contributing to LNO_x were considered for an unbiased comparison between the different thunderstorms.
[6] The LNO_x production rate per LINET stroke, see Eq. (2).
[7] The LINET stroke to LIS flash ratio for AMMA was 0.77.

we used the LINET stroke rate between 11:00–12:00 UTC (0.041 strokes s^{-1}). We believe that this number is representative for the selected penetrations in Table 3 (P5-6, P8-9) for several reasons. The satellite images show that the most active phase of the MCS was between midnight and 08:00 UTC. Between 09:00–14:00 UTC the storm slowly decayed. From Fig. 11a it is clear, that the stroke rate was not changing much between 11:00 and 14:00 UTC. We therefore do not expect a very different stroke rate at the beginning of the flight between 10:00–11:00 UTC, where no LINET stroke measurements were available. In addition, from the position and movement of the storm, we do not expect to observe a lot of aged NO (from older strokes) in the area where the penetrations took place. The analyses of WWLLN data for the region covered by the MCS (11–17° N, 0–6° E) indicate that the WWLLN stroke rate also rapidly decreased in the morning (07:00–08:00/08:00–09:00/09:00–10:00/10:00–11:00/11:00–12:00/12:00–13:00 UTC: 59/53/38/8/11/2 strokes s^{-1}) (R. Buergesser, FaMAF, Universidad Nacional de Cordoba, personal communication, 2011). Mainly the strokes between 10:00–12:00 UTC (from position and timing) contributed to the NO enhancement observed. Since the WWLLN stroke rate was almost constant between 10:00–12:00 UTC, we may assume that the selected LINET stroke rate between 11:00–12:00 UTC (0.041 strokes s^{-1}) is representative for our selected penetrations listed in Table 3.

On 15 August, we focus on the flight segments located closest to the convective core with fresh lightning (flight segments 5 to 6). Here the mean ambient wind velocity during 4 min before flight segment 5 and after flight segment 6 was determined together with its standard deviation (σ). The whole lifecycle of the stroke activity, until the selected flight segments were probed, was then divided into 30-min intervals. For each of these intervals it was determined which of the strokes, located upstream of the penetration, could be advected with the mean ambient wind velocity $\pm\sigma$ to the location of the penetration. Here again only strokes with peak currents $\geq$10 kA were taken into account. With the mean ambient wind velocity of 9 ± 2 m s^{-1} it was estimated that about 951 strokes between 12:00 and 16:00 UTC, located within the area 1.1–2.7° E, could have contributed to the measured anvil-NO_x in flight segments 5 to 6. This gives an average stroke rate of 0.066 strokes s^{-1}. Between 13:00 and 14:30 UTC, the time period when most strokes contributed to anvil-NO_x, the mean height of the IC strokes was estimated to 8.2 ± 2.9 km. The upper range ~8–11 km is partly located within the MCS outflow region investigated by the aircraft (~10–12 km).

The stroke rates R_{LINET} estimated for these two selected AMMA MCS on 6 and 15 August (~0.04 and ~0.07 strokes s^{-1}, respectively) are in a similar range as observed during TROCCINOX: 0.03 strokes s^{-1} for a subtropical thunderstorm and 0.05–0.06 strokes s^{-1} for selected tropical thunderstorms, and during SCOUT-O3: 0.04 to 0.11 strokes s^{-1} for selected tropical thunderstorms (except Hector) and 0.13 strokes s^{-1} for a subtropical thunderstorm (HH08; HH09). In comparison, in Hector stroke rates up to 0.24 strokes s^{-1} were observed.

For each of the selected MCS, the width Δx of the LNO_x plume perpendicular to the wind direction was estimated from the horizontal extension of enhanced anvil-NO_x and the LINET stroke distribution in Fig. 10a and b. This value is needed for further calculations according to Eq. (1). The Δx values obtained are ~220 km for the SLMCS on 6 August, and ~150 km for the MCS on 15 August, as listed in Table 3. These values are much higher than observed during TROCCINOX and SCOUT-O3 with Δx values in the range of ~30–60 km, except for Hector with ~100 km (HH08; HH09). For further calculations for AMMA, only the flight segments close to the convective core were selected (Table 3). For the 6 August case, no LINET strokes were

recorded north of ∼13.5° N within the MCS, since this area was out of range of the detection system. Therefore, only flight segments influenced by the coloured LINET strokes in Fig. 10a were considered.

4.2 Contribution of boundary layer (BL)-NO_x to anvil-NO_x

The NO_x mixing ratio measured in the fresh MCS outflow is mainly a mixture of LNO_x and NO_x transported upward from the BL with convection (BL-NO_x). In our previous studies (Huntrieser et al., 2002; HH08), the BL contribution to the NO_x mixing ratio in the anvil was derived from the correlation between NO_x and CO mixing ratios in the BL and in the anvil. It is assumed, that BL air is transported upwards rapidly within strong, well-developed updrafts by the convection, with little ambient mixing and without chemical loss of NO_x and CO in the first stage. In Sect. 5 we discuss this is more detail.

The vertical NO_x profile obtained from the Falcon measurements on 6 August indicates that mixing ratios in the range of 0.1–0.2 nmol mol^{-1} were present at the top of the BL (here ∼1.5 km altitude). Furthermore, we use the NO_x-CO scatter correlation plot from the whole flight to estimate the contribution from BL-NO_x to the measured anvil-NO_x in the outflow (not shown). During the selected flight segments listed in Table 3, CO mixing ratios in the range of ∼100–105 nmol mol^{-1} were measured (Table 2a). The average BL-NO_x mixing ratio $\chi_{\text{BL-NO}_x}$ for this CO-range, if we exclude NO_x mixing ratios above 0.25 nmol mol^{-1} (affected by LNO_x), is 0.16 ± 0.05 nmol mol^{-1}. This range is in accordance to our estimate from the vertical NO_x profile.

For the selected flight on 15 August no observations of NO_x were available at the top of the BL (assumed 0.8–1.2 km). Measurements from other AMMA-flights in this region at altitudes below 900 hPa generally indicate NO_x mixing ratios <0.4 nmol mol^{-1} (Reeves et al., 2010). Here, we use the NO_x-CO scatter correlation plot from this flight to estimate the contribution from BL-NO_x to the measured anvil-NO_x in the outflow (Fig. 12). During the selected flight segments listed in Table 3, CO mixing ratios in the range of ∼135–140 nmol mol^{-1} were measured (Table 2a). The average BL-NO_x mixing ratio $\chi_{\text{BL-NO}_x}$ for this CO-range, if we exclude NO_x mixing ratios above 0.30 nmol mol^{-1} (affected by LNO_x), is 0.18 ± 0.04 nmol mol^{-1}.

Average LNO_x volume mixing ratios χ_{LNO_x} were determined by subtraction of the mean BL-NO_x contribution $\chi_{\text{BL-NO}_x}$ (0.16 and 0.18 nmol mol^{-1}, respectively) from the mean anvil-NO_x values. The mean values for anvil-NO_x varied between 0.33–0.35 nmol mol^{-1}. As a result, χ_{LNO_x} values from 0.16 to 0.19 nmol mol^{-1} were obtained, as listed in Table 3. These χ_{LNO_x} values are distinctly lower compared to results from TROCCINOX and SCOUT-O3, where χ_{LNO_x} values ranged from 0.1 to 1.1 and from 0.4 to 2.4 nmol mol^{-1}, respectively (HH08; HH09).

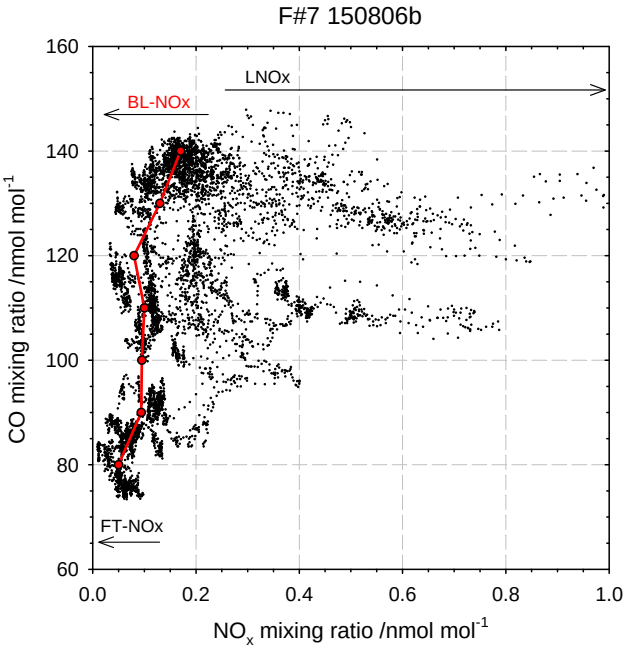

Fig. 12. NO_x-CO correlation plot for the Falcon b-flight on 15 August 2006. The NO_x contributions from the free troposphere (FT), boundary layer (BL) and from production by lightning (LNO_x) are indicated. The red line indicates the changing NO_x contribution from the BL and FT depending on CO mixing ratios.

Overall, the contribution of BL-NO_x to anvil-NO_x in the selected MCS of 6 and 15 August, was in the range of ∼50% (Table 3). This range is distinctly higher, than the average contributions found in European (EULINOX) thunderstorms with ∼25 to 40% (Huntrieser et al., 1998, 2002), in Brazilian (TROCCINOX) thunderstorms with ∼10 to 20% (HH08), and in Australian (SCOUT-O3) thunderstorms with less than 10% (HH09). During SCOUT-O3, the contribution from LNO_x clearly dominated the anvil-NO_x budget (≥90%), which indicates that the Darwin region is especially suitable for investigations of LNO_x.

4.3 Estimate of the mean depth of the anvil outflow

The mean depth of the anvil outflow Δz is needed as the next parameter for estimating the horizontal LNO_x mass flux in Eq. (1). For tropical regions it has been proposed, that the level of maximum anvil outflow and convective detrainment of O_3-poor air from the BL is located where minimum O_3 mixing ratios are observed (Folkins et al., 2002; Folkins and Martin, 2005). The mean vertical O_3 profile obtained from all Geophysica flights during AMMA indicates that the main anvil outflow region, characterised by especially low O_3 mixing ratios, was located between 9 and 13 km altitude, with a minimum centered around 12 km (Fig. 13). In agreement, Cetrone and Houze (2009) reported that anvils originating from MCS over West Africa are in general located at

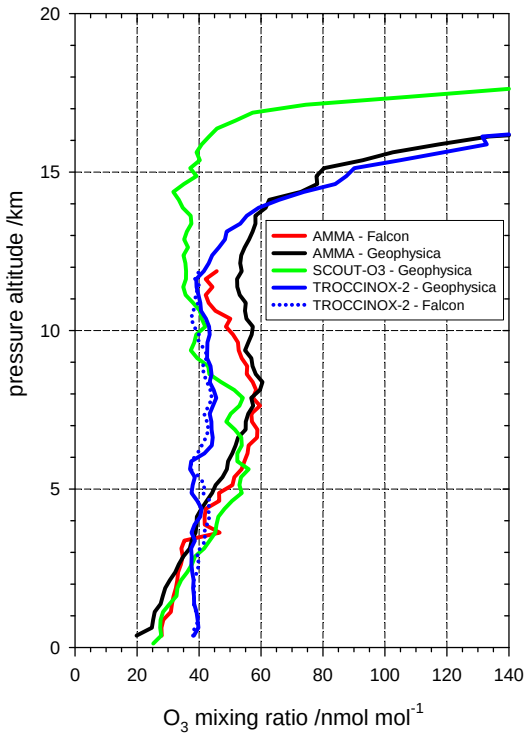

Fig. 13. Mean vertical O_3 profiles derived from measurements with the Falcon (flights 01b/04/06/07/11/13/15a–b/16/18a August 2006) and Geophysica (flights 04/07/08/11/13/16/17 August 2006) during AMMA. Superimposed are mean vertical O_3 profiles from SCOUT-O3 and TROCCINOX-2 (adapted from HH07; HH09). Mean values were calculated for every 250 m altitude bin.

~12 km altitude. Law et al. (2010) confined the altitude of maximum convective outflow in this region to 12.5 km based on observations of the vertical distribution of the cloud presence and by using the definition by Gettelman et al. (2004) based on the height of the 350 K level. In comparison, during SCOUT-O3 the main anvil outflow region was located higher up, between 11 and 15 km, according to the Geophysica O_3 measurements (HH09).

To estimate the vertical dimensions Δz of the anvil outflows, a combination of Falcon measurements including vertical profiles of the equivalent-potential temperature (Θ_e), wind velocity, O_3, and CO mixing ratios were used. For the computation of Θ_e for a water-saturation pseudo-adiabatic process, the formula developed by Bolton (1980) was used for Falcon data (see also HH07). Furthermore, Dessler (2002) has used a combination of the latter two chemical indicators to infer the convective outflow in the tropics. During AMMA, the main convective outflow was usually located at potential temperature levels up to ~350–360 K (13–14 km) according to Homan et al. (2010), coincident with the base of the TTL and the maximum level of neutral buoyancy.

On 6 August, O_3 mixing ratios distinctly decreased above ~9 km and reached values down to ~35–40 nmol mol^{-1} in the main anvil outflow, however at the top of the BL even lower mixing ratios in the range of ~25 nmol mol^{-1} were observed (Fig. 5a, Table 2a). The anvil outflow region is less distinct in the vertical CO profile. The CO mixing ratios are slightly enhanced above ~9 km and reach values in the range of ~100–110 nmol mol^{-1}, similar to the values at the top of the BL (1.5 km).

Since no other airborne measurements were available above 12 km for this day and for the 15 August (see below), the top of the anvil outflow region was estimated from the vertical Θ_e profile. Highwood and Hoskins (1998) and Folkins et al. (2000) have suggested that the upper level of the outflow is located where the Θ_e value is in the same range as observed at the top of the BL. The vertical Θ_e profile from 6 August indicates, that the maximum Θ_e temperature observed at the top of the BL (~350 K) is reached again in the UT at ~12 km (Fig. 5d). Based on these observations, we assume that the mean depth of the main anvil outflow on 6 August reached from ~9–12 km and Δz is ~3 km (Table 3).

On 15 August, the airborne measurements within the MCS also indicate that outflow signatures were clearly visible first above 10 km, with a decrease in O_3 mixing ratios down to ~30–40 nmol mol^{-1} and a distinct increase in CO mixing ratios up to ~120–150 nmol mol^{-1} (Fig. 9a, Table 2b). In this case more the typical "mirroring" of trace gas conditions (CO and O_3) in the BL and in the anvil outflow region was observed (Fig. 9a). An extrapolation of the vertical Θ_e profile from 15 August indicates that the maximum Θ_e temperature observed at the top of the BL (~355 K) is reached again in the UT at ~12.5 km (Fig. 9d). Based on these observations, we assume that the mean depth of the main anvil outflow on 15 August reached from ~10.0–12.5 km and Δz is ~2.5 km (Table 3). In this region (up to 11 km) also a large part of the IC strokes were released, as mentioned in Sect. 4.1.

4.4 Estimate of the horizontal LNO_x mass flux

For the final calculations of the horizontal LNO_x mass flux, it is also important to know if the selected MCS were penetrated in a comparable and representative way. The anvil penetrations listed in Table 3 provide only snapshots of the conditions at a certain level of the cloud at a certain time. These are, however, the only measurements available, and the most representative anvil penetrations were selected for Table 3. Furthermore, in the previous sections it was shown that the selected penetrations levels were located well within the main anvil outflow region and close to the region where most signals from IC strokes were registered.

Based on the parameters estimated in the previous sections and summarised in Table 3, the horizontal LNO_x mass flux F_{LNO_x} (in nitrogen mass per time, g s^{-1}) was calculated according to Eq. (1) for the selected anvil penetrations. The F_{LNO_x} values ranged from 85 to 140 g s^{-1}, which is within

the range estimated for TROCCINOX thunderstorms, 48–178 g s^{-1} (HH08). In comparison, for the Hector thunderstorm during SCOUT-O3 much higher F_{LNO_x} values up to ~700 g s^{-1} were estimated (HH09).

The fluxes given in Table 3 can be divided by the molar mass for nitrogen and the area of the vertical cross-section ($\Delta x \cdot \Delta z$) to estimate the flux in units of mol m^{-2} s^{-1}. For the selected AMMA thunderstorms, these fluxes vary between 1.4 and 1.6×10^{-8} mol m^{-2} s^{-1}. This is a distinctly smaller range than found for TROCCINOX and SCOUT-O3 thunderstorms with values between 3.3 and 7.1×10^{-8} mol m^{-2} s^{-1} and between 2.6 and 20.8×10^{-8} mol m^{-2} s^{-1}, respectively (HH08; HH09). However, due to the small number of thunderstorms available, it is not known how representative these values are. The values can also be compared to nitrogen mass fluxes simulated by Barth et al. (2007), who ran different cloud-scale models and achieved 2.7–13.0×10^{-8} mol m^{-2} s^{-1}, and to Barthe et al. (2007), who simulated 6×10^{-8} mol m^{-2} s^{-1} on average in the anvil outflow of a STERAO storm.

The parameters listed in Table 3 have large uncertainties. The relative maximum error of the F_{LNO_x} estimate was therefore calculated, defined as the sum of the single relative errors. The uncertainty for χ_{LNO_x} is given by the standard deviation (on average ~40% of the mean value); for V_a the standard deviations indicate an uncertainty of ~30% and for V_s the uncertainty is ~2 m s^{-1} corresponding to ~20%; for Δx and Δz the uncertainties were ~50–100 km and ~0.5–1 km, respectively, corresponding to uncertainties up to ~50% and ~40%. Summing up these uncertainties, the relative maximum error of the F_{LNO_x} estimate is ~180%.

4.5 Estimate of the LNO_x production rate per stroke and per year

For the estimate of the LNO_x production rate P_{LNO_x} (nitrogen mass per stroke, in g stroke^{-1}), the horizontal LNO_x mass flux F_{LNO_x} (g s^{-1}) is divided by the LINET stroke rate R_{LINET} (strokes s^{-1}) according to Eq. (2). Here only stronger LINET strokes with peak currents ≥10 kA were considered as mentioned before in Sect. 2.3. P_{LNO_x} estimates for the selected anvil penetrations resulted in values ranging from ~1.3 kg stroke^{-1} for the MCS on 15 August, located south of the ITCZ, and up to ~3.4 kg stroke^{-1} for the MCS on 6 August, located north of the ITCZ (Table 3).

For comparison with other published results, the P_{LNO_x} estimates per LINET stroke were scaled to P_{LNO_x} estimates per LIS flash. We are aware of the fact that a LINET stroke is not directly comparable to a LIS flash. Here we only use this LINET stroke – LIS flash relationship for scaling purposes. During the AMMA field phase, during daytime only one TRMM satellite overpass on 14 August (13:12:51–13:14:44 UTC) provided a sufficient large set of coincident LIS flash observations within the LINET domain. Lightning activity between the LINET centre area and the northern periphery, covering totally 10.2 to 12.6° N and 0.4 to 2.9° E, was suitable for comparison. During this selected overpass overall 89 LIS flashes and 94 LINET strokes with peak currents ≥10 kA were registered in this area. For the selected time period, Fig. 14 shows the horizontal distributions of all available LINET strokes and LIS flashes for the area where lightning occurred. The LIS detection efficiency for daytime (0.73) was taken into account for the LIS overpasses. This implies a LINET/LIS ratio of about $(94/89) \times 0.73 = 0.77$ for the selected overpass, considering only LINET strokes with peak currents ≥10 kA.

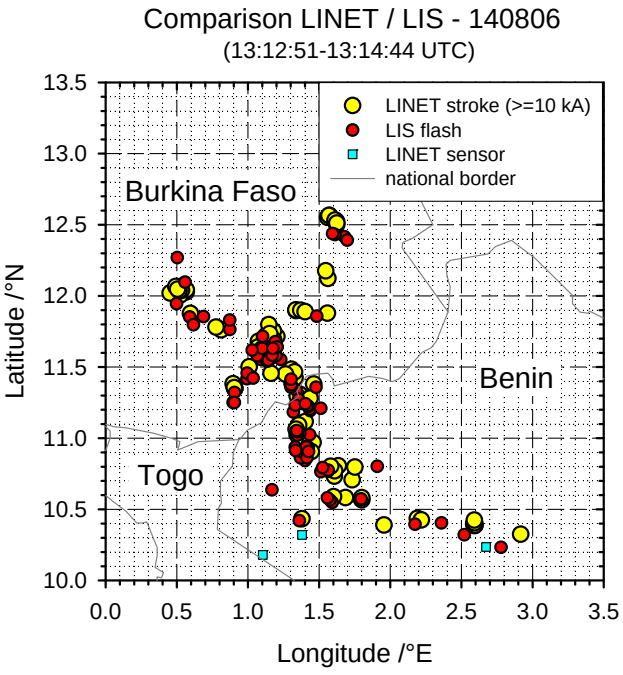

Fig. 14. Horizontal distributions of LIS flashes (in red) and LINET strokes with peak currents ≥10 kA (in yellow) during the LIS overpass over the LINET area on 14 August 2006. Close-by detecting LINET sensors are superimposed (in cyan).

By means of this ratio, the mean value for P_{LNO_x} per LIS flash for the MCS on 6 and 15 August was 2.5 and 1.0 kg, respectively (Table 3). This tendency to lower LNO_x production rates in regions closer to the tropics was also observed during TROCCINOX and SCOUT-O3 (HH08; HH09). The mean nitrogen production rates per LIS flash in tropical and subtropical thunderstorms during TROCCINOX was 1.2 and 2.2 kg, respectively. During SCOUT-O3, on average 1.5 kg was observed in smaller tropical thunderstorms, however in subtropical thunderstorms and Hector values ranged up to ~4–5 kg. Possible reasons for these differences will be discussed later in Sect. 7. These values obtained from AMMA are well within the range of values given in a review of previous investigations, where SH07 derived a best-estimate of 3.5 (range 0.5–10) kg of nitrogen per flash. The mean values for P_{LNO_x} per LIS flash given in Table 3 correspond

Table 4. Comparison of different parameters influencing LNO_X based on results from the field campaigns AMMA (West Africa), TROCCINOX (Brazil) and SCOUT-O3 (North Australia), with values partly adapted from Huntrieser et al. (2007, 2008, 2009).

Field experiment, flight/latitude	Mean O_3 mixing ratio in 7–8 km, nmol mol^{-1}	R^2_{LINET}, (LINET strokes) s^{-1}	Δx, km	Δz, km	Mean $\chi^3_{BL\text{-}NO_x}$, nmol mol^{-1}	Mean $\chi^4_{LNO_x}$, nmol mol^{-1}	Ratio $\chi_{BL\text{-}NO_x}$ to χ_{LNO_x}, %	Ratio NO/NO_y	$\lvert V_a - V_s \rvert^5$, m s^{-1}	$F^6_{LNO_x}$, g(N) s^{-1}	$F^6_{LNO_x}$, $\times 10^{-8}$ mol m^{-2} s^{-1}	$P^7_{LNO_x}$, kg(N) (LIS flash)$^{-1}$	$P^7_{LNO_x}$, $\times 10^{25}$ molecules NO (LIS flash)$^{-1}$	$G^8_{LNO_x}$, Tg(N) a^{-1}
AMMA 060806 (13–15° N)	~50–60	0.04	~220	~3	0.16	0.2	~50/50	0.3	7	135	1.4	2.5	10.8	3.5
AMMA 150806b (9–10° N)	~60–70	0.07	~150	~2–3	0.18	0.2	~50/50	0.3	9	85	1.6	1.0	4.3	1.4
SCOUT-O3 (Hector)[1] (11–15° S)	~50–60	0.04–0.13 (<0.24)	~30–60 (<95)	~1–3	0.13	0.4–2.3 (<2.4)	~10/90	0.6–0.8 (<0.8)	5–15 (<8)	30–426 (<700)	2.6–20.3 (<20.8)	1.3–5.4 (<4.7)	5.6–23.2 (<20.2)	1.8–7.6 (<6.6)
TROCCINOX (19–22° S)	~40–50	0.03–0.06	~30–50	~3–4	0.11	0.1–1.1	~20/80	0.3–0.8	6–20	48–178	3.3–7.1	1.0–2.8	4.3–12.0	1.3–3.9
	mean tropical[9]													~2
	mean subtropical[9]													~4
	mean all (range)													~3 **(1–8)**

[1] For SCOUT-O3, values in brackets are given for the Hector thunderstorm.

[2] Only LINET strokes with peak currents ≥10 kA contributing to LNO_X were considered for an unbiased comparison between the different thunderstorms.

[3] Mean NO_X mixing ratio transported from the boundary layer (BL-NO_X) into the anvil outflow.

[4] Mean NO_X mixing ratio produced by lightning (LNO_X) in the anvil outflow (difference between total measured anvil-NO_X and the BL-NO_X contribution).

[5] True horizontal anvil outflow velocity (difference between the wind vectors in the anvil outflow and at the steering level).

[6] The horizontal LNO_X mass flux out of the anvil, see Eq. (1).

[7] The LNO_X production rate per LIS flash, see Eq. (2).

[8] The annual global LNO_X production rate, see Sect. 4.

[9] The mean for tropical and subtropical thunderstorms was estimated from all selected tropical and subtropical thunderstorm penetrations from TROCCINOX (as listed in HH08), from SCOUT-O3 (as listed in HH09), and from AMMA based on the 060806 case (subtropical) and 150806b case (tropical) listed above.

to a total range of 4.3–10.8 × 10^{25} molecules NO per LIS flash. This range is very similar to the range observed during TROCCINOX with 4.3–12.0 × 10^{25} molecules NO (HH08). In comparison, during SCOUT-O3 a total range of 5.6–23.2 × 10^{25} molecules NO was estimated, which implies a factor ~2 higher production rates in thunderstorms in the Darwin region compared to AMMA and TROCCINOX (Table 4). SH07 concluded that a typical flash produces 15(2–40) × 10^{25} molecules NO. Our results from TROCCINOX and AMMA are located below this global mean value.

The different estimates for AMMA, SCOUT-O3 and TROCCINOX thunderstorms may be influenced by the different LINET/LIS ratios obtained (~0.8, 1.6, and 0.5, respectively) (HH08; HH09). It is not clear why the LINET/LIS ratios during AMMA, SCOUT-O3 and TROCCINOX are so different. Since the LINET configuration was about the same on the investigated AMMA, SCOUT-O3 and TROCCINOX days (4–5 stations were active and the average distance to the next closest sensor was ~80–90 km), we assume that the LINET detection efficiency was similar for peak currents ≥10 kA. However, we speculate that the number of LINET strokes ≥10 kA per LIS flash or the LIS detection efficiency for IC and CG flashes may be different. Results by Höller et al. (2009) indicate an elevated fraction of LINET strokes ≥10 kA for Australia compared to Brazil and Benin, which may explain our different LINET/LIS ratios. Furthermore, Petersen and Rutledge (1992) pointed out that especially high mean peak currents in negative CG flashes were observed over Northern Australia compared to other regions.

The AMMA estimates for P_{LNO_x} per LIS flash were finally multiplied with the number of LIS flashes occurring globally, 44 flashes s^{-1}. If we assume that the selected AMMA thunderstorms were representative for the globe, the implied mean annual global LNO_x production rate G_{LNO_x} based on the two MCS on 6 and 15 August, would be 3.5 and 1.4 Tg a^{-1}, respectively (Table 3). This range is again similar to the mean values obtained for subtropical and tropical thunderstorms during TROCCINOX, 3.1 and 1.6 Tg a^{-1}, respectively (HH08). However, compared to the mean values obtained for different SCOUT-O3 thunderstorms (range 2.4–7.6 Tg a^{-1}), these values are distinctly lower (HH09).

Finally, the relative maximum errors of the P_{LNO_x} and G_{LNO_x} estimates (Table 3) were calculated. The uncertainty for R_{LINET} was estimated from the ratio between total strokes occurring in the cell and the number of strokes considered to have contributed to LNO_x (uncertainty range ~60%). From the estimates for F_{LNO_x} ~180% and R_{LINET} ~60%, the relative maximum error of the P_{LNO_x} estimate for LINET strokes was ~240%. For the P_{LNO_x} estimate for LIS flashes, it was assumed that the uncertainty in the conversion of LINET strokes (≥10 kA) to LIS flashes was ~50% (depending on uncertainties in LIS and LINET detection efficiencies). This gives a relative maximum error of ~290%. For the G_{LNO_x} estimate, the uncertainty in the global LIS flash rate was given with ~10%, which gives a final relative maximum error of ~300%. Considering this relative maximum error, G_{LNO_x} values listed in Table 3 may range up to ~14 Tg a^{-1}, which is within the range of up to ~20 Tg a^{-1} given for G_{LNO_x} in previous assessments (e.g., WMO, 1999; SH07).

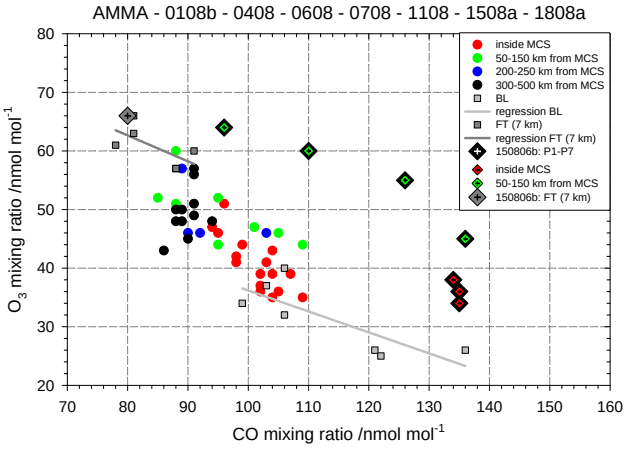

Fig. 15. CO-O_3 correlations during single penetrations of MCS outflow on selected AMMA Falcon flights 2006 as indicated in the header and legend. Flights listed in the header are represented by dots in different colours depending on the distance from the MCS. Superimposed are the correlations in the free troposphere (FT) and boundary layer (BL) for the selected flights in the header and their regressions (dark and light grey squares). The flight listed in the legend (150806b) is represented by a black diamond superimposed by smaller coloured diamonds depending on the distance from the MCS. The grey diamond represents the correlation in the FT for this flight.

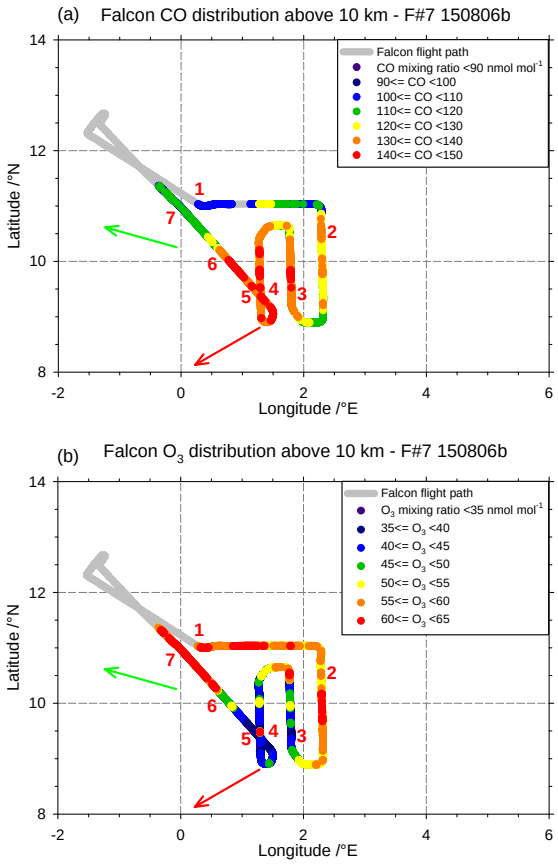

Fig. 16. Distribution of CO **(a)** and O_3 **(b)** mixing ratios along the Falcon flight path above 10 km on 15 August 2006. The selected flight segments are labelled. The red arrow indicates the direction of the storm motion and the green arrow the main wind direction in the anvil outflow (not scaled according to velocity).

5 Production, destruction or mixing of O_3 in the MCS outflow?

In our selected AMMA cases, the observed O_3 mixing ratios in the fresh MCS outflow were distinctly lower than in the ambient air and attributed to direct airmass transport from the O_3-poor BL (Sects. 3.2 and 3.3). In addition, Bechara et al. (2010) observed O_3 mixing ratios in the range of 45 nmol mol^{-1} within the fresh MCS outflow during AMMA compared to 60 nmol mol^{-1} outside. As the MCS outflow ages, the O_3 composition in the MCS outflow may be affected both by photochemical O_3 production/destruction of uplifted precursors and mixing with the ambient air (Chatfield and Delany, 1990). For selected AMMA cases, Ancellet et al. (2009) found that the chemical reactivity and O_3 production in the MCS outflow are related to the lifetime of the MCS, the position and chemical composition of the ingested airmasses. Ozone production rates in the range of 1 nmol mol^{-1} per hour have been calculated for the outflow from MCS during AMMA (Andrés-Hernández et al., 2009). In convective outflow impacted by LNO_x, ozone production rates in the range of 5–10 nmol mol^{-1} per day have been reported from previous campaigns in the tropics and midlatitudes (Pickering et al., 1996; Fehr et al., 2004; DeCaria et al., 2005; Ott et al., 2007).

In Table 2a and b it was shown that the trace gas composition observed in the fresh MCS outflow was rather different on 6 and 15 August, with higher mixing ratios of CO and HCHO for the latter flight. In addition, during the mixing with the ambient air further downwind, O_3 mixing ratios increased much faster in the aged MCS outflow on 15 August. In this section, we discuss these findings in more detail by analysing the O_3/CO correlation in different MCS outflows as a function of distance from the convective core.

To achieve a clearer picture, all available penetrations in the fresh and aged MCS outflow (within ~500 km distance) during the whole AMMA SOP-2a2 period were analysed. Data from the following flights were used: 1(b), 4, 6, 7, 11, 15(a–b), and 18(a) August 2006. The mean CO and O_3 mixing ratios were determined for all penetrations in the MCS outflow. In addition, the distance to the convective core was estimated from MSG satellite images. The data set was divided into 4 categories: inside MCS, in 50–150, 200–250, and 300–500 km distance from the convective core. Furthermore, mean CO and O_3 mixing ratios for the boundary layer (BL) and the free troposphere (FT) below the convective outflow, here taken to be ~7 km, were determined for all the selected flights. The vertical O_3 profiles (Fig. 13) indicate that

the region above 8 km is affected by the convective outflow O_3 mixing ratios decrease) and therefore not suitable as typical background. In Fig. 15, the O_3/CO correlation for this selected data set (39 points in the MCS outflow) is shown together with BL and FT conditions. The data from the 15 August b-flight was treated in a separate way, due to the different observations mentioned before and since it was the only flight investigating MCS south of the ITCZ (∼10° N).

The O_3/CO correlations from all selected MCS outflows (flight 15b excluded) show a very similar picture (Fig. 15). The correlations obtained in the fresh (aged) outflow are located close to the conditions in the BL (FT), respectively. The data points are arranged along a rather straight mixing line between the BL and FT. With increasing distance from the convective core, CO and O_3 mixing ratios in the MCS outflow decrease and increase, respectively, in a way expected from mixing with the ambient FT air. From this correlation plot it is hard to recognise if O_3 production takes place in the aged MCS outflow (here within ∼500 km distance). The mixing with the ambient FT air seems to be the most prevailing process that changes the mixing ratios. At a distance of 300–500 km from the core, CO mixing ratios in the outflow almost achieve ambient FT conditions, however O_3 mixing ratios are still slightly lower (∼10 nmol mol^{-1}), indicating perhaps even some O_3 destruction at this early stage.

In comparison, for the b-flight from 15 August, where a MCS south of the ITCZ was investigated, the conditions are very different (Fig. 15). First of all, it is not known if the BL conditions in the Ouagadougou area are also representative for the BL below the investigated MCS over Northern Benin-Togo. Therefore, no information on the BL conditions for this flight is given in Fig. 15. The FT conditions for this flight (from Ouagadougou ascent/descent), are within the range of the previous flights. As mentioned before, CO mixing ratios were distinctly higher in the fresh MCS outflow on 15 August (b-flight) with ∼135 nmol mol^{-1} compared to the other selected fresh MCS outflows with a given range of ∼90–110 nmol mol^{-1}. Ozone mixing ratios were rather low (∼35–40 nmol mol^{-1}) and located within the lower range given from other fresh MCS outflows.

The observations in the aging outflow from the 15 August (b-flight), indicate a very steep increase in O_3 mixing ratios without much change in CO mixing ratios in the first phase (Fig. 15). The increase in O_3 mixing ratios with distance is however too strong to be attributed to O_3 production alone. Instead, probably mixing with the ambient air south of 10° N (known to be impacted by aged biomass burning plumes rich in O_3 and CO) primarily caused this rapid O_3 increase. In this case, perhaps also other important O_3 precursors as isoprene were transported upward from the polluted BL, since more isoprene producing vegetation is prominent in this tropical region compared to the region north of the ITCZ (Bechara et al., 2010; Reeves et al., 2010). At a distance of 100–150 km from the convective core, the mean O_3 mixing ratios reached ∼60–65 nmol mol^{-1}, which is distinctly higher

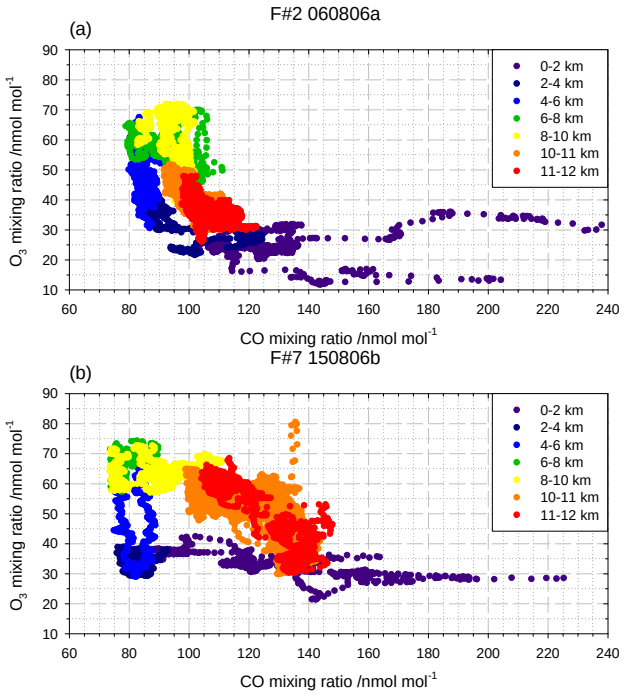

Fig. 17. CO-O_3 correlation plot for the AMMA flights on 6 August 2006 **(a)** and 15 August **(b)** (pressure altitude colour-coded).

(∼10–15 nmol mol^{-1}) compared to observations in the other MCS aged outflows north of the ITCZ (∼45–55 nmol mol^{-1}) at this distance.

In Fig. 16a and b the distributions of O_3 and CO mixing ratios along the flight path on 15 August above 10 km are shown. In the fresh outflow, close to the convective core (segment 3–5), CO and O_3 mixing ratios are distinctly enhanced and reduced, respectively, compared to the rest of the flight. In the aged convective outflow, along the rear side of the MCS, CO mixing ratios have slightly decreased, however O_3 mixing ratios have increased dramatically. Possible explanations for this increase were mentioned above. For the flight on 15 August, the aged outflow downwind of the MCS was probed in detail in flight segments 6 to 7 at ∼11.7 km altitude (north of 10° N). The outflow was probed as far as ∼130 km downwind of the MCS, thereafter the aircraft started to descend for landing. According to the ambient wind velocity (∼10 m s^{-1}) it was estimated that the most aged outflow probed by the aircraft, left the MCS ∼3–4 h earlier. In this aged outflow, signatures in NO were still clearly enhanced in comparison to ambient mixing ratios, O_3 mixing ratios remained high, however CO mixing ratios rapidly decreased due to the successive mixing with the less polluted airmass north of 10° N.

The differences in the trace gas composition between the 6 and 15 August flights are also clearly visible in Fig. 17a, b, respectively. Here all O_3/CO data points from the two flights are plotted and coloured according to pressure altitude. In

the UT (10–12 km), large differences in the O_3/CO correlation are visible between the two flights, as mentioned before. On 6 August, mixing of the fresh MCS outflow (with high CO and low O_3) with the ambient air is visible. With increasing age the data points move along the mixing line between the BL and FT. On 6 August, the data points in the upper MCS outflow region, at 10–12 km, coincide with data points located at ∼2 km, which means that the MCS inflow region was rather elevated on this day (see Sect. 4.2). In comparison, on 15 August the data points in 10–12 km altitude coincide with data points located distinctly lower probably at ∼1 km, which contain much more CO (Fig. 17b).

6 Brief synthesis of AMMA, SCOUT-O3 and TROCCINOX results concerning O_3 and LNO_x

The results from the AMMA field experiment concerning O_3 and LNO_x, were partly compared to SCOUT-O3 and TROCCINOX results in the course of this paper. For a better overview, these comparisons are summarised in Table 4.

First, the mean O_3 mixing ratios in 7–8 km, located just below the main anvil outflow, were compared (see Table 4 and Fig. 13). The highest ambient O_3 mixing ratios in the mid-upper troposphere (MUT) were observed during AMMA, indicative of the highest O_3 producing potential in this region. Here frequent intrusions of airmasses impacted by biomass burning from the Southern Hemisphere followed by convective uplift may contribute to enhance MUT O_3 mixing ratios (Sauvage et al., 2005, 2007; Barret et al., 2008; Mari et al., 2008; Ancellet et al., 2009; Real et al., 2010; Reeves et al., 2010). During AMMA, one of these elevated fire plumes from the south was also penetrated by the aircraft as far north as ∼5° N (Real et al., 2010). Mixing ratios as high as 450 nmol mol^{-1} CO, 130 nmol mol^{-1} O_3 and 8 nmol mol^{-1} NO_y were measured during this DLR Falcon flight. In these elevated fire plumes, photochemical O_3 formation rates up to 7 nmol mol^{-1} per day have been estimated during AMMA (Real et al., 2010). During other seasons even values up to 15–35 nmol mol^{-1} per day have been reported (Jonquières et al., 1998). In comparison, during TROCCINOX mean O_3 mixing ratios in the MUT were in general much lower and we observed no indication of a strong O_3 potential at these altitudes.

Second, different parameters influencing LNO_x were compared. As shown in Table 4, the range for the LINET stroke rates was rather similar during all three campaigns, however with a tendency to higher values during SCOUT-O3, especially for the intense Hector thunderstorm. This thunderstorm type was also wider than most other thunderstorms in the tropics and falls into the category MCS. The largest MCS were however observed during AMMA, where also the BL was slightly more polluted and the ratio of BL-NO_x to total anvil-NO_x was highest. During AMMA, the lowest LNO_x mixing ratios and NO/NO_y ratios were observed, indicative of only a minor contribution from LNO_x to anvil-NO_x. However, due to the large size of the AMMA-MCS, the LNO_x mass flux (in g s^{-1}) from these thunderstorms was in a similar range as for TROCCINOX, however distinctly lower than for SCOUT-O3 thunderstorms. In comparison, for SCOUT-O3 thunderstorms the highest production rate of nitrogen per LIS flash was determined. During AMMA, the lowest LNO_x production rate per flash (P_{LNO_x}) was observed in the MCS located south of the ITCZ in a more typical tropical airmass, which agrees with our previous observations during TROCCINOX and SCOUT-O3 (HH08; HH09). If we consider Hector thunderstorms to be typical global thunderstorms, an annual global production rate of up to ∼8 Tg(N) a^{-1} from lightning would be achieved. However, if we consider more typical tropical and subtropical thunderstorms observed during the three field campaigns, an annual global production rate of ∼2 and ∼4 Tg(N) a^{-1}, respectively, is obtained. A general tendency to higher production rates in the subtropics was observed. The influence from the higher wind shear in subtropical compared to the tropical regions was discussed in detail in HH08 and HH09. Further important parameters influencing LNO_x are discussed in the next Sect. 7. The overall mean for the annual global LNO_x production rate based on results from the AMMA, SCOUT-O3 and TROCCINOX field campaigns, was ∼3 Tg(N) a^{-1}, with a most likely range of ∼1–8 Tg(N) a^{-1}.

7 Recommendations for future LNO_x parameterisations based on results from AMMA, SCOUT-O3, TROCCINOX and other studies

As mentioned in the introduction, the parameterisation of LNO_x in models still requires substantial improvements to better agree with observations of NO_x and O_3. In the last years, a number of publications have contributed to improve our knowledge about the different processes affecting the LNO_x production that will be discussed briefly in this section. However, it is urgently needed to also incorporate these new findings into novel LNO_x parameterisations.

To explain the differences in P_{LNO_x} observed during AMMA, SCOUT-O3 and TROCCINOX, it would also be important to analyse additional parameters that might impact LNO_x. For example, the thermodynamic surface conditions were different during these campaigns (see also HH07 and HH09), with higher surface-Θ_e temperatures during SCOUT-O3 (∼355 K) compared to the other two campaigns (∼350 K) impacting the convective available potential energy (CAPE). In the next paragraphs below, it is explained why this and other parameters are crucial for LNO_x estimates. In our future LNO_x studies, we plan to focus more closely on the ice and graupel volume mass in thunderclouds and to use more detailed radar and lightning information as explained below.

One explanation for the high LNO_x production rates observed in the Hector thunderstorm during SCOUT-O3 may be related to the exceptional wide vertical extension of the volume containing large ice and graupel particles in the cloud (radar reflectivity >35–40 dBZ), reaching up to ~12–16 km (HH09; Höller et al., 2009). The importance of the graupel distribution and updraft velocities for lightning initiation, structure and flash rates has been pointed out by e.g., Zipser (1994); Zipser and Lutz (1994); Toracinta et al. (2002); and Wiens et al. (2005). Deierling and Petersen (2008) found that "large updraft volumes of "higher" updraft speeds are capable of producing more hydrometeors in the mixed ice phase region and thus higher number of collisions (between graupel and ice crystals) with subsequent charge separation". Lund et al. (2009) observed that most lightning in convective clouds over Oklahoma was initiated within the 35 dBZ radar contour containing graupel and within one of the two charge centres located between 3–6 km (positive/negative) or 7–10 km (positive/negative).

Observational, laboratory and model studies indicate that discharges preferably propagate into the cloud regions containing higher charge densities and that branching of the discharge increases in these regions, e.g. in the upper positive charge region (Williams, 1985; Mansell et al., 2002; Wiens et al., 2005; Cooray et al., 2009). For AMMA and TROCCINOX thunderstorms, the 35–40 dBZ radar reflectivity height was in general located lower compared to observations in Hector (Höller et al., 2009). Due to the fact that the vertical extension of graupel and large ice particles may be reduced, we hypothesize that the branching of each discharge was also reduced. This type of reduced discharge extension has been observed by e.g., Bruning et al. (2007) in the initial thunderstorm stage when cloud lightning only occurs within the lower positive and negative charge centre, before later flashes also propagate into the upper charge centre.

It is known that the LNO_x production per discharge is proportional to the channel length (Wang et al., 1998). Recent model studies by Cooray et al. (2009) indicate that the major contribution to NO_x is produced by the electrical activity within the cloud (5–10 km altitude). Mainly slow discharge processes play an important role for the NO_x production as the highly branched leaders (~50% contribution), continuing currents, and M components (impulsive processes, that occur during the continuing current following return strokes). The contribution to NO_x from return strokes is in comparison almost negligible (<10%), as also observed from measurements in triggered lightning by Rahman et al. (2007). We therefore hypothesize, that due to the reduced vertical extension of elevated radar reflectivity (>35–40 dBZ) observed in the AMMA and TROCCINOX cases referred to above, the LNO_x production per flash was also reduced in comparison to e.g., Hector during SCOUT-O3. Reduced vertical extension of elevated radar reflectivity has been observed in deep convective clouds with reduced vertical velocity and reduced environmental CAPE (Rutledge et al., 1992; Williams et al., 1992). During AMMA, it was observed that most MCS propagating along 8–16° N proceeded in an environment with relatively low CAPE, caused by the monsoon flow (Nieto Ferreira et al., 2009).

For MCS hot spot regions, Zipser et al. (2006) observed a distinct difference in ice scattering signatures (85- and 37-GHz brightness temperatures) between the MCS in South-central United States, Southeast South America and the Sahel zone. Similar cloud top heights (85-GHz brightness temperatures, generated by small precipitation sized ice, e.g., few hundred microns) and 20-dBZ radar echo-top heights were observed in all three regions, however the 37-GHz brightness temperatures above MCS in the Sahel zone were in general higher compared to the other two regions. The 37-GHz signal is attributed to the presence of larger (millimetre sized) graupel or frozen raindrops in convective cores (Toracinta et al., 2002). These observations indicate that 30- and 40-dBZ radar echo-top heights in Sahelian MCS were located lower (at higher temperatures) compared to the other two MCS hot spot regions. Furthermore, radar measurements from the Benin area carried out during AMMA confirm that the 40-dBZ level was in general observed at lower altitudes <5–6.5 km (Evaristo et al., 2010).

In the tropics in general, e.g., Toracinta et al. (2002) observed that for a given radar echo-top height of 20 dBZ, the vertical extension of the 30–40 dBZ layer is deeper in continental convection compared to maritime convection. Due to the influence of the monsoon, the radar features of the Sahelian MCS seem to be in a mixed stage between typical tropical continental convection and maritime convection. During the monsoon season in the Amazon basin, Williams et al. (2002) even observed typical tropical maritime radar signatures in the deep continental convection and termed the Amazon basin the "green ocean". In deep convection in the Darwin area, Rutledge et al. (1992) also observed distinct differences in vertical radar reflectivity and lightning activity during the monsoon (more maritime type) and break periods (more continental type) even for clouds with similar radar echo-tops. Recently, Futyan and Del Genio (2007b) found a second order power-law relationship between the lightning flash rate and the mean radar echo top height above the 0 °C isotherm (valid both for the radar reflectivity threshold >17 dBZ and >30 dBZ). This is the first relationship of its kind, which captures both the land-ocean contrast and regional differences in lightning occurrence, as between Africa, the Amazon, and the islands of the maritime continent.

In future studies to improve LNO_x parameterisations, we therefore highly recommend to incorporate the vertical extent of the important ice charged cloud region. The extension of the rainout zone and mixed phase zone in deep convection are important parameters that affect the microphysics and determines the amount of supercooled liquid water and graupel available in the upper part of the cloud (Rosenfeld and Lensky, 1998). Recently, Ott et al. (2010) distributed

LNO_x uniformly within the 20 dBZ contour computed from simulated hydrometeor fields in a cloud-scale model. Further improvements may perhaps be achieved, if we focus more on the vertical extension of the 35–40 dBZ region in the cloud, which has been found to affect the lightning activity substantially, as suggested by e.g., Toracinta et al. (2002) and Xu et al. (2010). Based on observations, Deierling et al. (2008) found a high correlation between lightning frequency and the product of the downward mass flux of solid precipitation (graupel) and the upward mass flux if ice crystals, which they suggested to incorporate in future LNO_x parameterisations. Furthermore, they suggested that "flash frequency that is *weighted by the flash lengths* or the power emitted by flashes may be more representative of the amount of charge equalized by a flash and should be looked at in future research". Recent findings by Cooray et al. (2009) indicate that the length of the lightning discharge channel inside the cloud is the most influencing parameter for the estimation of the global LNO_x rate. In addition, HH08 and HH09 also pointed out the importance of this length as explanation for different LNO_x amounts per flash observed in different types of continental thunderclouds (tropical/subtropical) during TROCCINOX and SCOUT-O3. Furthermore, in our previous analyses in tropical regions we also discussed the possible influence from the different stroke peak current distributions and mean stroke heights distributions (HH08, Höller et al., 2009).

Furthermore, parameters as CAPE, surface-Θ_e, convective inhibition (CIN), cloud base height (CBH), freezing level (0 °C), updraft velocity, wind shear and aerosol loading are all parameters that affect the intensity of the thunderstorm, lightning characteristics and finally LNO_x, and that should be (and partly have been) considered in LNO_x parameterisations (e.g., Zipser and LeMone, 1980; Szoke and Zipser, 1986; Szoke et al. 1986; Petersen and Rutledge, 1992; Rutledge et al., 1992; Williams et al., 1992; Toracinta et al., 2002; Williams et al., 2002; Choi et al., 2005; Mushak et al., 2005; Pickering et al., 2009; Altaratz et al., 2010; Kelley et al., 2010). Up to recently, the majority of all LNO_x parameterisations were related to *external* cloud properties as convective cloud top height (CTH), with different relationships for the continent/ocean used to simulate the global lightning distributions (Price and Rind, 1992). In the last years, improved LNO_x parameterisations have been proposed based on e.g. convective precipitation and upward convective mass flux (Allen et al., 2000; Grewe et al., 2001; Meijer et al., 2001; Allen and Pickering, 2002). Furthermore, Barthe and Pinty (2007) and Barthe et al. (2007) developed an explicit 3-D electrical scheme for LNO_x parameterisation in cloud resolving models. Recently, Barthe et al. (2010) have conducted cloud resolving model simulations to examine the correlation between the observed flash rate and six model parameters (precipitation ice mass, ice water path, ice mass flux product, updraft volume, maximum vertical velocity, and cloud top height). They found that the maximum vertical velocity and the precipitation ice mass correlate best with the flash rate. Good results were also achieved with the lightning potential index (LPI) which is a function of the condensate mixing ratios and the vertical velocity between 0 and $-20°$ C (Yair et al., 2010). For future LNO_x parameterisations, it would be important to preferably consider microphysical processes *within* the cloud or parameters influencing these processes, as explained above. For many regional and global models this is a challenge up to date.

Our results for the lightning-LNO_x production rate, based on field experiments in the tropics, are located at the lower end of the values used in most regional and global model studies (see e.g. Hudman et al., 2007; Jourdain et al., 2010; Ott et al., 2010). In addition, our results are located at the lower end of Fig. 28 in the review article by SH07. However, Fig. 28 is mainly based on model results. We believe that the main reason for these differences between model studies and our studies is that the model studies are based on midlatitude storm observations and our studies focus on thunderstorms in tropical regions. A recent study by Beirle et al. (2010), based on NO_2 column densities from SCIAMACHY measurements, also indicate distinctly lower LNOx production rates (less than 1 Tg(N) a^{-1}) compared to model studies. The large uncertainty range in the estimate of global LNOx production rate therefore still remains. From our point of view, we need more observations of LNOx in different types of regions. These regional estimates of LNO_x production rate per flash may then be used in model studies to improve the regional and global estimates. For future observations of LNO_x it would also be important to investigate more cases of vigorous convection penetrating the tropopause, as frequently observed over e.g., Central Africa (Congo) (Liu and Zipser, 2005; Futyan and Del Genio, 2007a). Simultaneous measurements of radar reflectivity, lightning and NO_x distributions seem to be essential to achieve improvements in the parameterisation of LNO_x.

8 Summary and conclusions

In this study we presented measurements carried out over West Africa with the German research aircraft *Falcon* (and partly Russian M55 *Geophysica*) and with the LINET lightning location network during the AMMA field phase in August 2006. In this season, the monsoon was fully developed and specific wind regimes were prominent, as the African Easterly Jet (AEJ) in the lower and mid troposphere (∼3–5 km), and the Tropical Easterly Jet (TEJ) in the UT.

We focused our analyses on the chemical composition in the outflow of two large MCS probed on 6 and 15 August, located north and south of the ITCZ (∼10° N), respectively. Both MCS contained rather low amounts of NO_x produced by lightning (∼50% of total NO_x in the fresh outflow) compared to our previous observations in tropical regions during TROCCINOX and SCOUT-O3 (HH07; HH08; HH09). In the anvil outflow (∼10–12 km), the contribution from LNO_x was on average <0.2 nmol mol^{-1} (peak ∼1 nmol mol^{-1}) and

the contribution from the BL was in a similar range. The highest LNO_x mixing ratios were observed closest to the convective core and at the highest flight level (11.9 km). Above this level, much higher LNO_x mixing ratios are not expected, since the clouds only extended up to ∼13 km and the majority of IC strokes were observed below 11 km. During AMMA, the TEJ (core ∼13–14 km) probably prevented the clouds from growing higher.

In comparison to the huge extension of these MCS (several 100 km wide), the stroke rate (∼0.04–0.07 s^{-1}) was in the same range as observed in average tropical thunderstorms (∼30–50 km) during our previous campaigns (here only LINET strokes with peak currents ≥10 kA contributing to LNO_x were considered for an unbiased comparison with the other thunderstorms). The LNO_x mass flux (F_{LNO_x}) in the MCS outflow during AMMA was estimated to be in the range of ∼100 g(N) s^{-1}. Combined with the stroke rate, the LNO_x production rate per LINET stroke (P_{LNO_x}) was estimated to be ∼1.3 and ∼3.3 kg(N) for the MCS on 15 and 6 August, respectively. For a better comparison with other studies, LINET strokes were scaled with LIS flashes and a factor of 0.77 LINET strokes per LIS flash was estimated. These values then correspond to ∼1.0 and 2.5 kg(N) per LIS flash for the MCS on 15 and 6 August, respectively. If we assume, that our different MCS during AMMA are typically global thunderstorms (LIS flash rate ∼44 s^{-1}), the annual global LNO_x production rate (G_{LNO_x}) was estimated to be ∼1.4 and 3.5 Tg(N) a^{-1} based on these two different MCS (factor 2.5 difference). The range of the G_{LNO_x} values estimated here is located at lower range of 5 ± 3 Tg(N) a^{-1}, as given in SH07 as best present estimate of the annual global LNO_x production rate. The overall mean for G_{LNO_x} estimated from selected AMMA, SCOUT-O3 and TROCCINOX thunderstorms was ∼3 Tg(N) a^{-1}, with the most likely range of ∼1–8 Tg(N) a^{-1}. Especially the thunderstorms investigated during SCOUT-O3 (Northern Australia) produced high amounts of flashes and LNO_x.

During AMMA, the lowest LNO_x production rate per flash (P_{LNO_x}) was observed in the MCS located south of the ITCZ in a more typical tropical airmass, which agrees with our previous observations during TROCCINOX and SCOUT-O3 (HH08; HH09). In our previous studies it was argued, that these differences in P_{LNO_x} may partly be caused by the different vertical wind shear observed in tropical and subtropical airmasses. It was shown that P_{LNO_x} was in general positively correlated with the wind shear. In contrast to our previous observations in tropical and subtropical airmasses, the absolute value of the wind velocity difference between the anvil region and the steering level was rather similar for both presented cases from AMMA, as a result of the prevailing AEJ. The single velocity values in the anvil and steering level were however very different, on 6 August the wind velocity increased and on 15 August it decreased with altitude. In this case, the MCS with the higher wind velocity in the UT (located north of the ICTZ closer to the subtropics) also produced more LNO_x per flash, a tendency also observed during the TC4 field experiment by Bucsela et al. (2010). Our previous analyses also suggested that the different vertical wind shear impacts the flash length and therefore the LNO_x production rate per flash (HH08; HH09). Recently, Cooray et al. (2009) also found that *length of the lightning discharge channel* is the most influencing parameter for estimating the global LNO_x production rate.

To explain the differences in P_{LNO_x} observed during AMMA, SCOUT-O3 and TROCCINOX it would also be important to analyse additional parameters that might impact LNO_x. During AMMA, it was observed that most MCS propagating along 8–16° N proceeded in an environment with relatively low CAPE, caused by the monsoon flow (Nieto Ferreira et al., 2009). As a result, the 35–40 dBZ radar reflectivity height was in general located lower compared to observations in Hector (Höller et al., 2009). Radar measurements from the Benin area carried out during AMMA confirm that the 40-dBZ level was in general observed at lower altitudes <5–6.5 km (Evaristo et al., 2010). In our future LNO_x studies, we plan to focus more closely on the ice and graupel volume mass in thunderclouds and to use more detailed radar and lightning information. One explanation for the high LNO_x production rates observed in the Hector thunderstorm during SCOUT-O3 may be connected to the exceptional wide vertical extension of the volume containing large ice and graupel particles in the cloud, reaching up to ∼12–16 km according to radar data (HH09; Höller et al., 2009). As a result, highly branched lightning channels may originate, producing a high amount of LNO_x per flash.

In this study the influence of MCS on both the NO_x and O_3 distribution in the UT was studied in detail. It was shown that the dry Saharan air layer (SAL) located in ∼3–5 km plays a crucial role for the chemical composition of trace gases observed in the MCS outflow. North of the ITCZ (∼10° N) this layer capped the subjacent monsoon layer and prevented fresh BL emissions from being ingested into the MCS on 6 August. In comparison, the investigated MCS on 15 August was located south of the ITCZ over a different vegetation zone with increasing forest/shrub cover and further away from the SAL. In this case, the trace gas composition in the MCS outflow indicated that more fresh emissions were transported upward directly from the BL (higher CO and HCO mixing ratios). In the fresh outflow, O_3 mixing ratios were almost as low as observed in the inflow region in both cases (∼35 nmol mol^{-1}), due to efficient vertical transport within the MCS. As the outflow aged, mixing with the ambient air was the most prominent feature during the first hours. Especially, south of the ITCZ, where the free tropospheric composition is largely impacted by aged biomass burning plumes, the mixing with these O_3-rich airmasses enhanced O_3 mixing ratios in the MCS outflow very rapidly from ∼35 to 65 nmol mol^{-1} within 2–3 h.

From the findings presented in this paper, we get further evidence that the conditions in the BL are essential for the

chemical composition observed in the fresh and aged MCS outflow region, and later for the production of O_3. Furthermore, the injection height of the ingested emissions also seems to play an important role. For future field experiments we therefore recommend to also investigate the chemical composition in the MCS *inflow* region in more detail if we should learn more about the O_3 production in the MCS *outflow*. It would be important to find out more about which trace gases are most important for the O_3 production in the MCS outflow. Regions with biomass burning seem to play an important role. Furthermore, it would be important to follow the evolution of the trace gas composition in the aged MCS outflow as long as possible and perhaps to use additional artificial tracers for longer detection.

Appendix A

Vertical wind shear estimate

For the calculation of the horizontal LNO_x mass flux in Sect. 4.4, the difference between the wind vectors in the anvil outflow and at the steering level $V_a - V_s$ must be estimated. The values for V_a were determined from the mean wind velocity in the anvil outflow for the selected flight segments. The values for V_s were determined from the spatial LINET stroke evolution based on horizontal stroke distributions with a high temporal resolution of 10 min. For the MCS on 6 August, the value for V_a for the flight segments 5–6 was 13.1 m s^{-1} from a northeasterly direction (∼70°). For the flight segments 8–9 the value for V_a was rather similar with 12.3 m s^{-1} from an easterly direction (∼95°). The value for V_s was determined to be 6.5 m s^{-1} from a northeasterly direction (∼70°). The resulting differences $V_a - V_s$ (6.6 and 7.0 m s^{-1}, respectively) for these two flight segments are listed in Table 3. In comparison, for the MCS on 15 August the value for V_a for the flight segments 5–6 was slightly lower with 9.7 m s^{-1} from a southeasterly direction (∼105°) and the value for V_s was distinctly higher with 12.5 m s^{-1} from a northeasterly direction (∼60°). In this case, the wind velocity decreased with altitude and the wind direction changed more with altitude. The resulting difference $V_a - V_s$ (8.9 m s^{-1}) is again listed in Table 3.

Acknowledgements. Based on a French initiative, AMMA was built by an international scientific group and was funded by a large number of agencies, especially from France, the UK, the United States, and Africa. It has been a beneficiary of a major financial contribution from the European Community Sixth Framework Programme (AMMA-EU). Detailed information on scientific coordination and funding is available on the AMMA International website at http://www.amma-international.org. The measurements presented here were partially also funded by the DLR (Deutsches Zentrum für Luft- und Raumfahrt) and other AMMA partners. We thank the Falcon and Geophysica pilots, the engineers and scientists of the flight departments for the excellent support during the field phase. The LINET system was installed in the Benin area as a joint effort between DLR and the University Abomey Calavi (E. Houngninou, E. Lezinme). We greatly acknowledge L. Oswald (DLR) for making the LINET system operations possible, M. Zich (nowcast GmbH) for the system support, the IRD (L'Institut de recherché pour le developpement) and AOC (AMMA operation centre) staff in Cotonou for logistic help. We express our gratitude to the lightning team at MSFC-NASA for the access to the LIS data and Meteo France for the processing of the MSG data (http://aoc.amma-international.org/observation/satellite/). The authors wish to thank the World Wide Lightning Location Network (http://wwlln.net), a collaboration among over 50 universities and institutions, for providing the lightning location data used in this paper. ECMWF is acknowledged for permitting access to their data archives. Finally, we thank Martin Dameris (DLR), the two anonymous reviewers and the editor for their comments and suggestions, which greatly helped to improve the manuscript.

Edited by: C. Reeves

References

Allen, D., Pickering, K., Stenchikov, G., Thompson, A., and Kondo, Y.: A three-dimensional total odd nitrogen (NO_y) simulation during SONEX using a stretched-grid chemical transport model, J. Geophys. Res., 105, 3851–3876, doi:10.1029/1999JD901029, 2000.

Allen, D. J. and Pickering, K. E.: Evaluation of lightning flash rate parameterizations for use in a global chemical-transport model, J. Geophys. Res., 107(D23), 4711, doi:10.1029/2002JD002066, 2002.

Altaratz, O., Koren, I., Yair, Y., and Price, C.: Lightning response to smoke from Amazonian fires, Geophys. Res. Lett., 37, L07801, doi:10.1029/2010GL042679, 2010.

Ancellet, G., Leclair de Bellevue, J., Mari, C., Nedelec, P., Kukui, A., Borbon, A., and Perros, P.: Effects of regional-scale and convective transports on tropospheric ozone chemistry revealed by aircraft observations during the wet season of the AMMA campaign, Atmos. Chem. Phys., 9, 383–411, doi:10.5194/acp-9-383-2009, 2009.

Andrés-Hernández, M. D., Kartal, D., Reichert, L., Burrows, J. P., Meyer Arnek, J., Lichtenstern, M., Stock, P., and Schlager, H.: Peroxy radical observations over West Africa during AMMA 2006: photochemical activity in the outflow of convective systems, Atmos. Chem. Phys., 9, 3681–3695, doi:10.5194/acp-9-3681-2009, 2009.

Andrés-Hernández, M. D., Stone, D., Brookes, D. M., Commane, R., Reeves, C. E., Huntrieser, H., Heard, D. E., Monks, P. S., Burrows, J. P., Schlager, H., Kartal, D., Evans, M. J., Floquet, C. F. A., Ingham, T., Methven, J., and Parker, A. E.: Peroxy radical partitioning during the AMMA radical intercomparison exercise, Atmos. Chem. Phys., 10, 10621–10638, doi:10.5194/acp-10-10621-2010, 2010.

Arlander, D. W., Brüning, D., Schmidt, U., and Ehhalt, D. H.: The tropospheric distribution of formaldehyde during TROPOZ II, J. Atmos. Chem., 22, 251–268, 1995.

Avery, M., Twohy, C., McCabe, D., Joiner, J., Severance, K., Atlas, E., Blake, D., Bui, T. P., Crounse, J., Dibb, J., Diskin, G., Lawson, P., McGill, M., Rogers, D., Sachse, G., Scheuer, E., Thompson, A. M., Trepte, C., Wennberg, P., and Ziemke,

J.: Convective distribution of tropospheric ozone and tracers in the Central American ITCZ region: Evidence from observations during TC4, J. Geophys. Res., 115, D00J21, doi:10.1029/2009JD013450, 2010.

Baehr, J., Schlager, H., Ziereis, H., Stock, P., van Velthoven, P., Busen, R., Ström, J., and Schumann, U.: Aircraft observations of NO, NO_y, CO, and O_3 in the upper troposphere from 60° N to 60° S – Interhemispheric differences at midlatitudes, Geophys. Res. Lett., 30, 1598, doi:10.1029/2003GL016935, 2003.

Barret, B., Ricaud, P., Mari, C., Attié, J.-L., Bousserez, N., Josse, B., Le Flochmoën, E., Livesey, N. J., Massart, S., Peuch, V.-H., Piacentini, A., Sauvage, B., Thouret, V., and Cammas, J.-P.: Transport pathways of CO in the African upper troposphere during the monsoon season: a study based upon the assimilation of spaceborne observations, Atmos. Chem. Phys., 8, 3231–3246, doi:10.5194/acp-8-3231-2008, 2008.

Barret, B., Williams, J. E., Bouarar, I., Yang, X., Josse, B., Law, K., Pham, M., Le Flochmoën, E., Liousse, C., Peuch, V. H., Carver, G. D., Pyle, J. A., Sauvage, B., van Velthoven, P., Schlager, H., Mari, C., and Cammas, J.-P.: Impact of West African Monsoon convective transport and lightning NO_x production upon the upper tropospheric composition: a multi-model study, Atmos. Chem. Phys., 10, 5719–5738, doi:10.5194/acp-10-5719-2010, 2010.

Barth, M. C., Kim, S.-W., Wang, C., Pickering, K. E., Ott, L. E., Stenchikov, G., Leriche, M., Cautenet, S., Pinty, J.-P., Barthe, Ch., Mari, C., Helsdon, J. H., Farley, R. D., Fridlind, A. M., Ackerman, A. S., Spiridonov, V., and Telenta, B.: Cloud-scale model intercomparison of chemical constituent transport in deep convection, Atmos. Chem. Phys., 7, 4709–4731, doi:10.5194/acp-7-4709-2007, 2007.

Barthe, C. and Pinty, J.-P.: Simulation of a supercellular storm using a three-dimensional mesoscale model with an explicit lightning flash scheme, J. Geophys. Res., 112, D06210, doi:10.1029/2006JD007484, 2007.

Barthe, C., Pinty, J.-P., and Mari, C.: Lightning-produced NO_x in an explicit electrical scheme tested in a Stratosphere-Troposphere Experiment: radiation, aerosols, and ozone case study, J. Geophys. Res., 112, D04302, doi:10.1029/2006JD007402, 2007.

Barthe, C., Deierling, W., and Barth, M. C.: Estimation of total lightning from various storm parameters: A cloud-resolving model study, J. Geophys. Res., 115, D24202, doi:10.1029/2010JD014405, 2010.

Bechara, J., Borbon, A., Jambert, C., Colomb, A., and Perros, P. E.: Evidence of the impact of deep convection on reactive Volatile Organic Compounds in the upper tropical troposphere during the AMMA experiment in West Africa, Atmos. Chem. Phys., 10, 10321–10334, doi:10.5194/acp-10-10321-2010, 2010.

Beirle, S., Huntrieser, H., and Wagner, T.: Direct satellite observation of lightning-produced NO_x, Atmos. Chem. Phys., 10, 10965–10986, doi:10.5194/acp-10-10965-2010, 2010.

Bertram, T. H., Perring, A. E., Wooldridge, P. J., Crounse, J. D., Kwan, A. J., Wennberg, P. O., Scheuer, E., Dibb, J., Avery, M., Sachse, G., Vay., S. A., Crawford, J. H., McNaughton, C. S., Clarke, A., Pickering, K. E., Fuelberg, H., Huey, G., Blake, D. R., Singh, H. B., Hall, S. R., Shetter, R. E., Fried, A., Heikes, B. G., and Cohen, R. C.: Direct measurements of the convective recycling of the upper troposphere, Science, 315, 816–820, 2007.

Betz, H.-D., Schmidt, K., Oettinger, W. P., and Wirz, M.: Lightning detection with 3-D-discrimination of intracloud and cloud-to-ground discharges, Geophys. Res. Lett., 31, L11108, doi:10.1029/2004GL019821, 2004.

Betz, H.-D., Schmidt, K., Fuchs, B., Oettinger, W. P. and Höller, H.: Cloud lightning: Detection and utilization for total lightning measured in the VLF/LF regime, J. Lightning Res., 2, 1–17, http://www.jolr.org/, 2007.

Betz, H.-D., Schmidt, K., Laroche, P., Blanchet, P., Oettinger, W. P., Defer, E., Dziewit, Z., and Konarski, J.: LINET – An international lightning detection network in Europe, Atmos. Res., 91, 564–573, 2009.

Bhetanabhotla, M. N., Crowell, B. A., Coucouvinos, A., Hill, R. D., and Rinker, R. G.: Simulation of trace species production by lightning and corona discharge in moist air, Atmos. Environ., 19, 1391–1397, 1985.

Boccippio, D. J., Koshak, W. J., and Blakeslee, R. J.: Performance assessment of the tropical transient detector and lightning imaging sensor. Part I: Predicted diurnal variability, J. Atmos. Oceanic Technol., 19, 1318–1332, 2002.

Bolton, D.: The computation of equivalent potential temperature, Mon. Weather Rev., 108, 1046–1053, 1980.

Bruning, E. C., Rust, W. D., Schuur, T. J., MacGorman, D. R., Krehbiel, P. R., and Rison, W.: Electrical and polarimetric radar observations of a multicell storm in TELEX, Mon. Weather Rev., 135, 2525–2544, 2007.

Bucsela, E. J., Pickering, K. E., Huntemann, T. L., Cohen, R. C., Perring, A., Gleason, J. F., Blakeslee, R. J., Albrecht, R. I., Holzworth, R., Cipriani, J. P., Vargas-Navarro, D., Mora-Segura, I., Pacheco-Hernandez, A., and Laporte-Molina, S.: Lightning-generated NO_x seen by OMI during NASA's TC^4 experiment, J. Geophys. Res., 115, D00J10, doi:10.1029/2009JD013118, 2010.

Burpee, R.: The origin and structure of easterly waves in the lower troposphere of North Africa, J. Atmos. Sci., 29, 77–90, 1972.

Cairo, F., Pommereau, J. P., Law, K. S., Schlager, H., Garnier, A., Fierli, F., Ern, M., Streibel, M., Arabas, S., Borrmann, S., Berthelier, J. J., Blom, C., Christensen, T., D'Amato, F., Di Donfrancesco, G., Deshler, T., Diedhiou, A., Durry, G., Engelsen, O., Goutail, F., Harris, N. R. P., Kerstel, E. R. T., Khaykin, S., Konopka, P., Kylling, A., Larsen, N., Lebel, T., Liu, X., MacKenzie, A. R., Nielsen, J., Oulanowski, A., Parker, D. J., Pelon, J., Polcher, J., Pyle, J. A., Ravegnani, F., Rivière, E. D., Robinson, A. D., Röckmann, T., Schiller, C., Simes, F., Stefanutti, L., Stroh, F., Some, L., Siegmund, P., Sitnikov, N., Vernier, J. P., Volk, C. M., Voigt, C., von Hobe, M., Viciani, S., and Yushkov, V.: An introduction to the SCOUT-AMMA stratospheric aircraft, balloons and sondes campaign in West Africa, August 2006: rationale and roadmap, Atmos. Chem. Phys., 10, 2237–2256, doi:10.5194/acp-10-2237-2010, 2010.

Cetrone, J. and Houze, R. A.: Anvil clouds of tropical mesoscale convective systems in monsoon regions, Q. J. Roy. Meteor. Soc., 135, 305–317, doi:10.1002/qj.389, 2009.

Chameides, W. L., Stedman, D. H., Dickerson, R. R., Rusch, D. W., and Cicerone, R. J.: NO_x production in lightning, J. Atmos. Sci., 34, 143–149, 1977.

Chameides, W. L., Davis, D. D., Bradshaw, J., Rodgers, M., Sandholm, S., and Bai, D. B.: An estimate of the NO_x production rate in electrified clouds based on NO observations from the GTE/CITE 1 fall 1983 field operation, J. Geophys. Res., 92, 2153–2156, 1987.

Chatfield, R. B. and Crutzen, P. J.: Sulfur dioxide in remote oceanic air: Cloud transport of reactive precursors, J. Geophys. Res., 89, 7111–7132, 1984.

Chatfield, R. and Delany, A.: Convection links biomass burning to increased tropical ozone: however, models will tend to overpredict O_3, J. Geophys. Res., 95(D11), 18473–18488, 1990.

Choi, Y., Wang, Y., Zeng, T., Martin, R. V., Kurosu, T. P., and Chance, K.: Evidence of lightning NO_x and convective transport of pollutants in satellite observations over North America, Geophys. Res. Lett., 32, L02805, doi:10.1029/2004GL021436, 2005.

Christian, H. J., Blakeslee, R. J., Goodman, S. J., Mach, D. A., Stewart, M. F., Buechler, D. E., Koshak, W. J., Hall, J. M., Boeck, W. L., Driscoll, K. T., and Bocippio, D. J.: The Lightning Imaging Sensor, Proceedings of the 11th International Conference on Atmospheric Electricity, Guntersville, Alabama, 7–11 June 1999, 746–749, 1999.

Christian, H. J., Blakeslee, R. J., Boccippio, D. J., Boeck, W. L., Buechler, D. E., Driscoll, K. T., Goodman, S. J., Hall, J. M., Koshak, W. J., Mach, D. M., and Stewart, M. F.: Global frequency and distribution of lightning as observed from space by the Optical Transient Detector, J. Geophys. Res., 108, 4005, doi:10.1029/2002JD002347, 2003.

Christian, H. J. and Petersen, W.: Global lightning activity, Conference on Meteorological Applications of Lightning Data, 85th AMS Annual Meeting, San Diego, CA, 10–12 January, 2005.

Cifelli, R., Lang, T., Rutledge, S. A., Guy, N., Zipser, E. J., Zawislak, J., and Holzworth, R.: Characteristics of an african easterly wave observed during NAMMA, J. Atmos. Sci., 67, 3–25, 2010.

Cooray, V., Rahman, M., and Rakov, V.: On the NO_X production by laboratory electrical discharges and lightning, J. Atmos. Sol.-Terr. Phys., 71, 1877–1889, 2009.

Crumeyrolle, S., Tulet, P., Gomes, L., Garcia-Carreras, L., Flamant, C., Parker, D. J., Matsuki, A., Formenti, P., and Schwarzenboeck, A.: Transport of dust particles from the Bodl region to the monsoon layer - AMMA case study of the 9-14 June 2006 period, Atmos. Chem. Phys., 11, 479–494, doi:10.5194/acp-11-479-2011, 2011.

Crutzen, P. J.: The influence of nitrogen oxides on the atmospheric ozone content, Q. J. Roy. Meteor. Soc., 96, 320–327, 1970.

DeCaria, A. J., Pickering, K. E., Stenchikov, G. L., and Ott, L. E.: Lightning-generated NO_X and its impact on tropospheric ozone production: A three-dimensional modeling study of a Stratosphere-Troposphere Experiment: Radiation, Aerosols and Ozone (STERAO-A) thunderstorm, J. Geophys. Res., 110, D14303, doi:10.1029/2004JD005556, 2005.

Deierling, W. and Petersen, W. A.: Total lightning activity as an indicator of updraft characteristics, J. Geophys. Res., 113, D16210, doi:10.1029/2007JD009598, 2008.

Deierling, W., Petersen, W. A., Latham, J., Ellis, S., and Christian, H. J.: The relationship between lightning activity and ice fluxes in thunderstorms, J. Geophys. Res., 113, D15210, doi:10.1029/2007JD009700, 2008.

Dessler, A. E.: The effect of deep tropical convection on the tropical tropopause layer, J. Geophys. Res., 107(D3), 4033, doi:10.1029/2001JD000511, 2002.

Dickerson, R. R., Huffman, G. J., Luke, W. T., Nunnermacker, L. J., Pickering, K. E., Leslie, A. C. D., Lindsey, C. G., Slinn, W. G. N., Kelly, T. J., Daum, P. H., Delany, A. C., Greenberg, J. P., Zimmerman, P. R., Boatman, J. F., Ray, J. D. and Stedman, D. H.: Thunderstorms: An important mechanism in the transport of air pollutants, Science, 235, 460–465, 1987.

Doherty, R. M., Stevenson, D. S., Collins, W. J., and Sanderson, M. G.: Influence of convective transport on tropospheric ozone and its precursors in a chemistry-climate model, Atmos. Chem. Phys., 5, 3205–3218, doi:10.5194/acp-5-3205-2005, 2005.

Dufour, G., Wittrock, F., Camredon, M., Beekmann, M., Richter, A., Aumont, B., and Burrows, J. P.: SCIAMACHY formaldehyde observations: constraint for isoprene emission estimates over Europe?, Atmos. Chem. Phys., 9, 1647–1664, doi:10.5194/acp-9-1647-2009, 2009.

Evaristo, R., Scialom, G., Viltard, N., and Lemaître, Y.: Polarimetric signatures and hydrometeor classification of West African squall lines, Q. J. Roy. Meteor. Soc., 136(s1), 272–288, doi:10.1002/qj.561, 2010.

Fehr, T., Höller, H., and Huntrieser, H.: Model study on production and transport of lightning-produced NO_x in an EULINOX supercell storm, J. Geophys. Res., 109, D09102, doi:10.1029/2003JD003935, 2004.

Fishman, J., Solomon, S., and Crutzen, P. J.: Observational and theoretical evidence in support of a significant in situ photochemical source of tropospheric ozone, Tellus, 31, 432–446, 1979.

Folkins, I., Oltmans, S. J., and Thompson, A. M.: Tropical convective outflow and near surface equivalent potential temperatures, Geophys. Res. Lett., 27, 2549–2552, 2000.

Folkins, I., Braun, C., Thompson, A. M., and Witte, J.: Tropical ozone as an indicator of deep convection, J. Geophys. Res., 107, 4184, doi:10.1029/2001JD001178, 2002.

Folkins, I. and Martin, R. V.: The vertical structure of tropical convection and its impact on the budgets of water vapor and ozone, J. Atmos. Sci., 62, 1560–1573, 2005.

Fueglistaler, S., Dessler, A. E., Dunkerton, T. J., Folkins, I., Fu, Q., Mote, P. W.: The tropical tropopause layer, Rev. Geophys., 47, RG1004, doi:10.1029/2008RG000267, 2009.

Futyan, J. M. and Del Genio, A. D.: Deep convective system evolution over Africa and the tropical Atlantic, J. Climate, 20, 5041–5060, 2007a.

Futyan, J. M. and Del Genio, A. D.: Relationships between lightning and properties of convective cloud clusters, Geophys. Res. Lett., 34, L15705, doi:10.1029/2007GL030227, 2007b.

Gettelman, A., Forster, P. M. deF., Fujiwara, M., Fu, Q., Vomel, H., Gohar, L. K., Johanson, C., and Ammerman, M.: Radiation balance of the tropical tropopause layer, J. Geophys. Res., 109, D07103, doi:10.1029/2003JD004190, 2004.

Grewe, V., Brunner, D., Dameris, M., Grenfell, J. L., Hein, R., Shindell, D., and Staehelin, J: Origin and variability of upper tropospheric nitrogen oxides and ozone at northern mid-latitudes, Atmos. Environ., 35, 3421–3433, 2001.

Highwood, E. J. and Hoskins, B. J.: The tropical tropopause, Q. J. Roy. Meteor. Soc., 124, 1579–1604, 1998.

Hodges, K. I. and Thorncroft, C. D.: Distribution and statistics of african mesoscale convective weather systems based on the ISCCP meteosat imagery, Mon. Weather Rev., 125, 2821–2837, 1997.

Höller, H., Finke, U., Huntrieser, H., Hagen, M., and Feigl, C.: Lightning produced NO_X (LINOX) – experimental design and case study results, J. Geophys. Res., 104, 13911–13922, 1999.

Höller, H., Betz, H.-D., Schmidt, K., Calheiros, R. V., May, P.,

Houngninou, E., and Scialom, G.: Lightning characteristics observed by a VLF/LF lightning detection network (LINET) in Brazil, Australia, Africa and Germany, Atmos. Chem. Phys., 9, 7795–7824, doi:10.5194/acp-9-7795-2009, 2009.

Homan, C. D., Volk, C. M., Kuhn, A. C., Werner, A., Baehr, J., Viciani, S., Ulanovski, A., and Ravegnani, F.: Tracer measurements in the tropical tropopause layer during the AMMA/SCOUT-O3 aircraft campaign, Atmos. Chem. Phys., 10, 3615–3627, doi:10.5194/acp-10-3615-2010, 2010.

Houze, R. A.: Cloud Dynamics, Academic, San Diego, California, 573 pp., 1993.

Houze, R. A.: Mesoscale convective systems, Rev. Geophys., 42, RG4003, doi:10.1029/2004RG000150, 2004.

Hudman, R. C., Jacob, D. J., Turquety, S., Leibensperger, E. M., Murray, L. T., Wu, S., Gilliland, A. B., Avery, M., Bertram, T. H., Brune, W., Cohen, R. C., Dibb, J. E., Flocke, F. M., Fried, A., Holloway, J., Neuman, J. A., Orville, R., Perring, A., Ren, X., Ryerson, T. B., Sachse, G. W., Singh, H. B., Swanson, A., and Wooldridge, P. J.: Surface and lightning sources of nitrogen oxides in the United States: Magnitudes, chemical evolution, and outflow, J. Geophys. Res., 112, D12S05, doi:10.1029/2006JD007912, 2007.

Huntemann, T. and Pickering, K.: Cloud-resolving simulations of Hector during SCOUT-O3/ACTIVE: case 16 November 2005, in preparation, 2011.

Huntrieser, H., Schlager, H., Feigl, C., and Höller, H.: Transport and production of NO_x in electrified thunderstorms: Survey of previous studies and new observations at mid-latitudes, J. Geophys. Res., 103, 28247–28264, 1998.

Huntrieser, H., Feigl, C., Schlager, H., Schröder, F., Gerbig, C., van Velthoven, P., Flatøy, F., Théry, C., Petzold, A., Höller, H., and Schumann, U.: Airborne measurements of NO_x, tracer species and small particles during the European Lightning Nitrogen Oxides Experiment, J. Geophys. Res., 107(D11), 4113, doi:10.1029/2000JD000209, ACH5-1–ACH5-24, 2002.

Huntrieser, H., Heland, J., Schlager, H., Forster, C., Stohl, A., Aufmhoff, H., Arnold, F., Scheel, E., Campana, M., Gilge, S., Eixmann, R., and Cooper, O.: Intercontinental air pollution transport from North America to Europe: experimental evidence from airborne measurements and surface observations, J. Geophys. Res., 110, D01305, doi:10.1029/2004JD005045, 2005.

Huntrieser, H., Schlager, H., Roiger, A., Lichtenstern, M., Schumann, U., Kurz, C., Brunner, D., Schwierz, C., Richter, A., and Stohl, A.: Lightning-produced NO_x over Brazil during TROCCINOX: airborne measurements in tropical and subtropical thunderstorms and the importance of mesoscale convective systems, Atmos. Chem. Phys., 7, 2987–3013, doi:10.5194/acp-7-2987-2007, 2007.

Huntrieser, H., Schumann, U., Schlager, H., Höller, H., Giez, A., Betz, H.-D., Brunner, D., Forster, C., Pinto Jr., O., and Calheiros, R.: Lightning activity in Brazilian thunderstorms during TROCCINOX: implications for NO_x production, Atmos. Chem. Phys., 8, 921–953, doi:10.5194/acp-8-921-2008, 2008.

Huntrieser, H., Schlager, H., Lichtenstern, M., Roiger, A., Stock, P., Minikin, A., Höller, H., Schmidt, K., Betz, H.-D., Allen, G., Viciani, S., Ulanovsky, A., Ravegnani, F., and Brunner, D.: NO_x production by lightning in Hector: first airborne measurements during SCOUT-O3/ACTIVE, Atmos. Chem. Phys., 9, 8377–8412, doi:10.5194/acp-9-8377-2009, 2009.

Jacob, D. J., Heikes, B. G., Fan, S.-M., Logan, J. A., Mauzerall, D. L., Bradshaw, J. D., Talbot, R. W., Blake, D. R., and Sachse, G. W.: Origin of ozone and NO_x in the tropical troposphere: A photochemical analysis of aircraft observations over the South Atlantic basin, J. Geophys. Res., 101(D19), 24235–24250, 1996.

Janicot, S., Thorncroft, C. D., Ali, A., Asencio, N., Berry, G., Bock, O., Bourles, B., Caniaux, G., Chauvin, F., Deme, A., Kergoat, L., Lafore, J.-P., Lavaysse, C., Lebel, T., Marticorena, B., Mounier, F., Nedelec, P., Redelsperger, J.-L., Ravegnani, F., Reeves, C. E., Roca, R., de Rosnay, P., Schlager, H., Sultan, B., Tomasini, M., Ulanovsky, A., and ACMAD forecasters team: Large-scale overview of the summer monsoon over West Africa during the AMMA field experiment in 2006, Ann. Geophys., 26, 2569–2595, doi:10.5194/angeo-26-2569-2008, 2008.

Jenkins G. S. and Pratt, A.: Saharan dust, lightning and tropical cyclones in the eastern tropical Atlantic during NAMMA-06, Geophys. Res. Lett., 35, L12804, doi:10.1029/2008GL033979, 2008.

Jonquières, I., Marenco, A., Maalej, A., and Rohrer, F.: Study of ozone formation and trans-atlantic transport from biomass burning emissions over West Africa during the airborne campaigns TROPOZ I and TROPOZ II, J. Geophys. Res., 103(D15), 19059–19073, 1998.

Jourdain, L., Kulawik, S. S., Worden, H. M., Pickering, K. E., Worden, J., and Thompson, A. M.: Lightning NO_x emissions over the USA constrained by TES ozone observations and the GEOS-Chem model, Atmos. Chem. Phys., 10, 107–119, doi:10.5194/acp-10-107-2010, 2010.

Keenan, T. D. and Carbone, R. E.: A preliminary morphology of precipitation systems in tropical Northern Australia, Q. J. Roy. Meteor. Soc., 118, 283–326, 1992.

Kelley, O. A., Stout, J., Summers, M., and Zipser, E. J.: Do the tallest convective cells over the tropical ocean have slow updrafts?, Mon. Weather Rev., 138, 1651–1672, 2010.

Koike, M., Kondo, Y., Kita, K., Takegawa, N., Nishi, N., Kashihara, T., Kawakami, S., Kudoh, S., Blake, D., Shirai, T., Liley, B., Ko, M., Miyazaki, Y., Kawasaki, Z., and Ogawa, T.: Measurements of reactive nitrogen produced by tropical thunderstorms during BIBLE-C, J. Geophys. Res., 112, D18304, doi:10.1029/2006JD008193, 2007.

Kollias P., Miller, M. A., Johnson, K. L., Jensen, M. P., and Troyan, D. T.: Cloud, thermodynamic, and precipitation observations in West Africa during 2006, J. Geophys. Res., 114, D00E08, doi:10.1029/2008JD010641, 2009.

Laing, A. G. and Fritsch, J. M.: Mesoscale Convective Complexes in Africa, Mon. Weather Rev., 121, 2254–2263, 1993.

Laing, A. G. and Fritsch, J. M.: The global population of mesoscale convective complexes, Q. J. Roy. Meteor. Soc., 123, 389–405, doi:10.1002/qj.49712353807, 1997.

Laing, A. G., Fritsch, J. M., and Negri, A. J.: Contribution of Mesoscale Convective Complexes to rainfall in Sahelian Africa: estimates from geostationary infrared and passive microwave data, J. Appl. Meteorol., 38, 957–964, 1999.

Laing, A. G., Carone, R., Levizzani, V., and Tuttle, J.: The propagation and diurnal cycles of deep convection in Northern Tropical Africa, Q. J. Roy. Meteor. Soc., 134, 93–109, doi:10.1002/qj.194, 2008.

Laurent, H., D'Amato, N., and Lebel, T.: How important is the contribution of the mesoscale convective complexes to the Sahelian rainfall?, Phys. Chem. Earth, 23, 629–633, 1998.

Law, K. S., Fierli, F., Cairo, F., Schlager, H., Borrmann, S., Streibel, M., Real, E., Kunkel, D., Schiller, C., Ravegnani, F., Ulanovsky, A., D'Amato, F., Viciani, S., and Volk, C. M.: Air mass origins influencing TTL chemical composition over West Africa during 2006 summer monsoon, Atmos. Chem. Phys., 10, 10753–10770, doi:10.5194/acp-10-10753-2010, 2010.

Lawrence, M. G., von Kuhlmann, R., and Salzmann, M.: The balance of effects of deep convective mixing on tropospheric ozone, Geophys. Res. Lett., 30(18), 1940, doi:10.1029/2003GL017644, 2003.

Lay, E. H., Holzworth, R. H., Rodger, C. J., Thomas, J. N., Pinto, O., Jr., Dowden, R. L.: WWLL global lightning detection system: Regional validation study in Brazil, Geophys. Res. Lett., 31, L03102, doi:10.1029/2003GL018882, 2004.

Lebel, T., Diedhiou, A., and Laurent, H.: Seasonal cycle and interannual variability of the Sahelian rainfall at hydrological scales, J. Geophys. Res., 108(D8), 8389, doi:10.1029/2001JD001580, 2003.

Lebel, T., Parker, D. J., Flamant, C., Bourles, B., Marticorena, B., Mougin, E., Peugeot, C., Diedhiou, A., Haywood, J. M., Ngamini, J. B., Polcher, J., Redelsperger, J.-L., and Thorncroft, C. D.: The AMMA field campaigns: multiscale and multidisciplinary observations in the West African region, Q. J. Roy. Meteor. Soc., 136(S1), 8–33, doi:10.1002/qj.486, 2009.

Lelieveld, J. and Crutzen, P. J.: Role of deep cloud convection in the ozone budget of the troposphere, Science, 264, 1759–1761, 1994.

Liu, C. and Zipser, E. J.: Global distribution of convection penetrating the tropical tropopause, J. Geophys. Res., 110, D23104, doi:10.1029/2005JD006063, 2005.

Lund, N. R., MacGorman, D. R., Schuur, T. J., Biggerstaff, M. I., and Rust, W. D.: Relationships between lightning location and polarimetric radar signatures in a small mesoscale convective system, Mon. Weather Rev., 137, 4151–4170, 2009.

Maddox, R. A.: Mesoscale convective complexes, B. Am. Meteorol. Soc., 61, 1374–1387, 1980.

Mansell, E. R., MacGorman, D. R., Ziegler, C. L., and Straka, J. M.: Simulated three-dimensional branched lightning in a numerical thunderstorm model, J. Geophys. Res., 107, 4075, doi:10.1029/2000JD000244, 2002.

Mari, C. H., Cailley, G., Corre, L., Saunois, M., Attié, J. L., Thouret, V., and Stohl, A.: Tracing biomass burning plumes from the Southern Hemisphere during the AMMA 2006 wet season experiment, Atmos. Chem. Phys., 8, 3951–3961, doi:10.5194/acp-8-3951-2008, 2008.

Martin, R. V., Jacob, D. J., Logan, J. A., Bey, I., Yantosca, R. M., Staudt, A. C., Li, Q., Fiore, A. M., Duncan, B. N., Liu, H., Ginoux, P., and Thouret, V.: Interpretation of TOMS observations of tropical tropospheric ozone with a global model and in situ observations, J. Geophys. Res., 107, 4351, doi:10.1029/2001JD001480, 2002.

Martin, R. V., Sioris, C. E., Chance, K., Ryerson, T. B., Bertram, T. H., Wooldridge, P. J., Cohen, R. C., Neuman, J. A., Swanson, A., and Flocke, F. M.: Evaluation of space-based constraints on global nitrogen oxide emissions with regional aircraft measurements over and downwind of Eastern North America, J. Geophys. Res., 111, D15308, doi:10.1029/2005JD006680, 2006.

Martin, R. V., Sauvage, B., Folkins, I., Sioris, C. E., Boone, C., Bernath, P., and Ziemke, J.: Space-based constraints on the production of nitric oxide by lightning, J. Geophys. Res., 112, D09309, doi:10.1029/2006JD007831, 2007.

Mathon, V. and Laurent, H.: Life cycle of Sahelian mesoscale convective cloud systems, Q. J. Roy. Meteor. Soc., 127, 377–406, doi:10.1002/qj.49712757208, 2001.

Mathon, V., Laurent, H., and Lebel, T.: Mesoscale convective system rainfall in the Sahel. J. Appl. Meteorol., 41, 1081–1092, 2002.

Meijer, E. W., van Velthoven, P. F. J., Brunner, D. W., Huntrieser, H., and Kelder, H.: Improvement and evaluation of the parameterisation of nitrogen oxide production by lightning, Phys. Chem. Earth, 26, 577–583, 2001.

Mohr, K. I. and Zipser, E. J.: Mesoscale convective systems defined by their 85-GHz ice scattering signature: size and intensity comparison over tropical oceans and continents, Mon. Weather Rev., 124, 2417–2437, 1996.

Mushtak, V. C., Williams, E. R., and Boccippio, D. J.: Latitudinal variations of cloud base height and lightning parameters in the tropics, Atmos. Res., 76, 222–230, 2005.

Nicholson, S. E.: A revised picture of the structure of the "monsoon" and land ITCZ over West Africa, Clim. Dynam., 32, 1155–1171, 2009.

Nieto Ferreira, R., Rickenbach, T., Guy, N., and Williams, E.: Radar observations of convective system variability in relationship to African easterly waves during the 2006 AMMA Special Observing Period, Mon. Weather Rev., 137, 4136–4150, 2009.

Ott, L. E., Pickering, K. E., Stenchikov, G. L., Huntrieser, H., and Schumann, U.: Effects of lightning NO_x production during the July 21 European Lightning Nitrogen Oxides Project storm studied with a three-dimensional cloud-scale chemical transport model, J. Geophys. Res., 112, D05307, doi:10.1029/2006JD007365, 2007.

Ott, L. E., Pickering, K. E., Stenchikov, G. L., Allen, D., DeCaria, A., Ridley, B., Lin, R.-F., Lang, S., and Tao, W.-K.: Production of lightning NO_x and its vertical distribution calculated from three-dimensional cloud-scale chemical transport model simulations, J. Geophys. Res., 115, D04301, doi:10.1029/2009JD011880, 2010.

Parker, D. J., Burton, R. R., Diongue-Niang, A., Ellis, R. J., Felton, M., Taylor, C. M., Thorncroft, C. D., Bessemoulin, P., and Tompkins, A. M.: The diurnal cycle of the West African monsoon circulation, Q. J. Roy. Meteor. Soc., 131, 2839–2860, 2005a.

Petersen, W. A. and Rutledge, S. A.: Some characteristics of cloud-to-ground lightning in tropical Northern Australia, J. Geophys. Res., 97, 11553–11560, 1992.

Pickering, K. E., Thompson, A. M., Tao, W.-K., and Kucsera, T. L.: Upper tropospheric ozone production following mesoscale convection during STEP/EMEX, J. Geophys. Res., 98, 8737–8749, 1993.

Pickering, K. E., Thompson, A. E., Wang, Y., Tao, W.-K., McNamara, D. P., Kirchhoff, V. W. J. H., Heikes, B. G., Sachse, G. W., Bradshaw, J. D., Gregory, G. L., and Blake, D. R.: Convective transport of biomass burning emissions over Brazil during TRACE-A, J. Geophys. Res., 101, 23993–24012, 1996.

Pickering, K. E., Huntrieser, H. and Schumann, U.: Lightning and NO_x production in global models, In: Lightning: Principles, Instruments and Applications, Review of Modern Lightning Research, edited by: Betz, H. D., Schumann, U., and Laroche, P.,

Springer Verlag, 551–571, ISBN:978-1-4020-9078-3, 2009.

Price, C. and Rind, D.: A simple lightning parameterization for calculating global lightning distributions, J. Geophys. Res., 97, 9919–9933, 1992.

Rahman, M., Corray, V., Rakov, V. A., Uman, M. A., Liyanage, P., DeCarlo B. A., Jerauld, J., and Olsen III, R. C.: Measurements of NO_x produced by rocket-triggered lightning, Geophys. Res. Lett., 34, L03816, doi:10.1029/2006GL027956, 2007.

Real, E., Orlandi, E., Law, K. S., Fierli, F., Josset, D., Cairo, F., Schlager, H., Borrmann, S., Kunkel, D., Volk, C. M., McQuaid, J. B., Stewart, D. J., Lee, J., Lewis, A. C., Hopkins, J. R., Raveg-nani, F., Ulanovski, A., and Liousse, C.: Cross-hemispheric transport of central African biomass burning pollutants: implications for downwind ozone production, Atmos. Chem. Phys., 10, 3027–3046, doi:10.5194/acp-10-3027-2010, 2010.

Redelsperger, J. L., Thorncroft, C. D., Diedhiou, A., Lebel, T., Parker, D. J., and Polcher, J.: African monsoon multidisciplinary analysis: an international research project and field campaign, B. Am. Meteorol. Soc., 87(12), 1739–1746, doi:10.1175/BAMS-87-12-1739, 2006.

Reeves, C. E., Formenti, P., Afif, C., Ancellet, G., Attié, J.-L., Bechara, J., Borbon, A., Cairo, F., Coe, H., Crumeyrolle, S., Fierli, F., Flamant, C., Gomes, L., Hamburger, T., Jambert, C., Law, K. S., Mari, C., Jones, R. L., Matsuki, A., Mead, M. I., Methven, J., Mills, G. P., Minikin, A., Murphy, J. G., Nielsen, J. K., Oram, D. E., Parker, D. J., Richter, A., Schlager, H., Schwarzenboeck, A., and Thouret, V.: Chemical and aerosol characterisation of the troposphere over West Africa during the monsoon period as part of AMMA, Atmos. Chem. Phys., 10, 7575–7601, doi:10.5194/acp-10-7575-2010, 2010.

Richter, A. and Burrows, J. P.: Retrieval of tropospheric NO_2 from GOME measurements, Adv. Space Res., 29, 1673–1683, 2002.

Rickenbach, T., Nieto Ferreira, R., Guy, N., and Williams, E.: Radar-observed squall line propagation and the diurnal cycle of convection in Niamey, Niger, during the 2006 African Monsoon and Multidisciplinary Analyses Intensive Observing Period, J. Geophys. Res., 114, D03107, doi:10.1029/2008JD010871, 2009.

Roca, R., Lafore, J.-P., Piriou, C., and Redelsperger, J.-L.: Extratropical dry-air intrusions into the West African monsoon midtroposphere: An important factor for the convective activity over the Sahel, J. Atmos. Sci., 62, 390–407, 2005.

Rosenfeld, D. and Lensky, I. M.: Spaceborne sensed insights into precipitation formation processes in continental and maritime clouds, B. Am. Meteorol. Soc., 79, 2457–2476, 1998.

Rowell, D. P. and Milford, J. R.: On the generation of African squall lines, J. Climate, 6, 1181–1193, 1993.

Rutledge, S. A., Williams, E. R., and Keenan, T. D.: The Down-Under Doppler and Electricity Experiment (DUNDEE): overview and preliminary results, B. Am. Meteorol. Soc., 73, 3–16, 1992.

Saunders, C. P. R., Keith, W. D., and Mitzeva, R. P.: The effect of liquid water on thunderstorm charging, J. Geophys. Res., 96, 11007–11017, 1991.

Saunois, M., Reeves, C. E., Mari, C. H., Murphy, J. G., Stewart, D. J., Mills, G. P., Oram, D. E., and Purvis, R. M.: Factors controlling the distribution of ozone in the West African lower troposphere during the AMMA (African Monsoon Multidisciplinary Analysis) wet season campaign, Atmos. Chem. Phys., 9, 6135–6155, doi:10.5194/acp-9-6135-2009, 2009.

Sauvage, B., Thouret, V., Cammas, J.-P., Gheusi, F., Athier, G., and Nédélec, P.: Tropospheric ozone over Equatorial Africa: regional aspects from the MOZAIC data, Atmos. Chem. Phys., 5, 311–335, doi:10.5194/acp-5-311-2005, 2005.

Sauvage, B., Gheusi, F., Thouret, V., Cammas, J.-P., Duron, J., Escobar, J., Mari, C., Mascart, P., and Pont, V.: Medium-range mid-tropospheric transport of ozone and precursors over Africa: two numerical case studies in dry and wet seasons, Atmos. Chem. Phys., 7, 5357–5370, doi:10.5194/acp-7-5357-2007, 2007.

Schmidt, K., Betz, H.-D., Oettinger, W. P., Wirz, M., and Diendorfer, G.: A new lightning detection network in Southern Germany, 27th International Conference on Lightning Protection (ICLP), September 2004, Avignon, France, 2004.

Schmidt, K., Betz, H.-D., Oettinger, W. P., Wirz, M., Pinto Jr., O., Naccarato, K. P., Höller, H., Fehr, T., and Held, G.: A comparative analysis of lightning data during the EU-Brazil TROCCINOX/TroCCiBras campaign, VIII International Symposium on Lightning Protection (SIPDA), 21–25 Nov 2005, São Paulo, Brazil, 2005.

Schmidt, K.: Ortung und Analyse von Blitzentladungen mittels Registrierung von VLF-Atmospherics innerhalb eines Messnetzes, Ph.D. thesis, Ludwig-Maximilians-Universität, Munich, Germany, 2007.

Schumann, U. and Huntrieser, H.: The global lightning-induced nitrogen oxides source, Atmos. Chem. Phys., 7, 3823–3907, doi:10.5194/acp-7-3823-2007, 2007.

Sioris, C. E., McLinden, C. A., Martin, R. V., Sauvage, B., Haley, C. S., Lloyd, N. D., Llewellyn, E. J., Bernath, P. F., Boone, C. D., Brohede, S., and McElroy, C. T.: Vertical profiles of lightning-produced NO_2 enhancements in the upper troposphere observed by OSIRIS, Atmos. Chem. Phys., 7, 4281–4294, doi:10.5194/acp-7-4281-2007, 2007.

Skamarock, W. C., Dye, J. E., Defer, E., Barth, M. C., Stith, J. L., Ridley, B. A., and, Baumann, K.: Observational- and modelling-based budget of lightning-produced NO_x in a continental thunderstorm, J. Geophys. Res., 108, 4305, doi:10.1029/2002JD002163, 2003.

Stefanutti, L., MacKenzie, A. R., Santacesaria, V., Adriani, A., Balestri, S., Borrmann, S., Khattatov, V., Mazzinghi, P., Mitev, V., Rudakov, V., Schiller, C., Toci, G., Volk, C. M., Yushkov, V., Flentje, H., Kiemle, C., Redaelli, G., Carslaw, K. S., Noone, K., and Peter, Th.: The APE-THESEO tropical campaign: an overview, J. Atmos. Chem., 48, 1–33, 2004.

Stevenson, D. S., Dentener, F. J., Schultz, M. G., Ellingsen, K., van Noije, T. P. C., Wild, O., Zeng, G., Amann, M., Atherton, C. S., Bell, N., Bergmann, D. J., Bey, I., Butler, T., Cofala, J., Collins, W. J., Derwent, R. G., Doherty, R. M., Drevet, J., Eskes, H. J., Fiore, A. M., Gauss, M., Hauglustaine, D. A., Horowitz, L. W., Isaksen, I. S. A., Krol, M. C., Lamarque, J.-F., Lawrence, M. G., Montanaro, V., Mueller, J.-F., Pitari, G., Prather, M. J., Pyle, J. A., Rast, S., Rodriguez, J. M., Sanderson, M. G., Savage, N. H., Shindell, D. T., Strahan, S. E., Sudo, K., and Szopa, S.: Multimodel ensemble simulations of present-day and near-future tropospheric ozone, J. Geophys. Res., 111, D08301, doi:10.1029/2005JD006338, 2006.

Szoke, E. J. and Zipser, E. J.: A radar study of convective cells in mesoscale systems in GATE. Part II: Life cycle of convective cells, J. Atmos. Sci., 43, 199–218, 1986.

Szoke, E. J., E. J. Zipser, and D. P. Jorgensen: A radar study of

convective cells in mesoscale systems in GATE. Part I: Vertical profile statistics and comparison with hurricanes, J. Atmos. Sci., 43, 182–198, 1986.

Takahashi, T.: Riming electrification as a charge generation mechanism in thunderstorms, J. Atmos. Sci., 35, 1536–1548, 1978.

Thomas, R. J., Krehbiel, P. R., Rison, W., Hamlin, T., Boccippio, D. J., Goodman, S. J., and Christian, H. J.: Comparison of ground-based 3-dimensional lightning mapping observations with satellite-based LIS observations in Oklahoma, Geophys. Res. Lett., 27, 1703–1706, 2000.

Thompson, A. M., Pickering, K. E., Dickerson, R. R., Ellis, Jr., W. G., Jacob, D. J., Scala, J. R., Tao, W. K., McNamara, D. P., and Simpson, J.: Convective transport over the central United States and its role in regional CO and ozone budgets, J. Geophys. Res., 99, 18703–18711, 1994.

Thompson, A. M., Tao, W. K., Pickering, K. E., Scala, J. R., and Simpson, J.: Tropical deep convection and ozone formation, B. Am. Meteorol. Soc., 78, 1043–1054, 1997.

Thorncroft, C. and Haile, M.: The mean dynamical and thermodynamic fields for July 1989 over tropical North Africa and their relationship to convective storm activity, Mon. Weather Rev., 123, 3016–3031, 1995.

Thorncroft, C. D., Parker, D. J., Burton, R. R., Diop, M., Hayers, J. H., Barjat, H., Dumelow, R., Kindred, D. R., Price, N. M., Taylor, C. M., and Tompkins, A. M.: The JET2000 Project: aircraft observations of the african easterly jet and african easterly waves, B. Am. Meteorol. Soc., 84, 337–351, 2003.

Toracinta, E. R., Cecil, D. J., Zipser, E. J., and Nesbitt, S. W.: Radar, passive microwave, and lightning characteristics of precipitating systems in the tropics, Mon. Weather Rev., 130, 802–824, 2002.

Tost, H., Jöckel, P., and Lelieveld, J.: Lightning and convection parameterisations – uncertainties in global modelling, Atmos. Chem. Phys., 7, 4553–4568, doi:10.5194/acp-7-4553-2007, 2007.

Volz-Thomas, A., Lerner, A., Pätz, H.-W., Schultz, M., McKenna, D. S., Schmitt, R., Madronich, S., and Röth, E. P.: Airborne measurements of the photolysis frequency of NO_2, J. Geophys. Res., 101, 18613–18627, 1996.

Wang, Y., DeSilva, A. W., and Goldenbaum, G. C.: Nitric oxide production by simulated lightning: Dependence on current, energy, and pressure, J. Geophys. Res., 103, 19149–19159, 1998.

Wiens, K. C., Rutledge, S. A., and Tessendorf, S. A.: The 29 June 2000 supercell observed during STEPS. Part II: Lightning and charge structure, J. Atmos. Sci., 62, 4151–4177, 2005.

Williams, E. R.: Electrical discharge propagation in and around space charge clouds, J. Geophys. Res., 90, 6059–6070, 1985.

Williams, E. R., Rutledge, S. A., Geotis, S. G., Renno, N., Rasmussen, E., and Rickenbach, T.: A radar end electrical study of tropical "hot towers", J. Atmos. Sci., 49, 1386–1395, 1992.

Williams, E., Rosenfeld, D., Madden, N., Gerlach, J., Gears, N., Atkinson, L., Dunnemann, N., Frostrom, G., Antonio, M., Biazon, B., Camargo, R., Franca, H., Gomes, A., Lima, M., Machado, R., Manhaes, S., Nachtigall, L., Piva, H., Quintiliano, W., Machado, L., and Artaxo, P.: Contrasting convective regimes over the Amazon: implications for cloud electrification, J. Geophys. Res., 107, 8082, doi:10.1029/2001JD000380, 2002.

WMO: Scientific Assessment of Ozone Depletion: 1998, World Meteorological Organisation, Geneva, Switzerland, 1999.

Xiao, Y., Jacob, D. J., and Turquety, S.: Atmospheric acetylene and its relationship with CO as an indicator of air mass age, J. Geophys. Res., 112, D12305, doi:10.1029/2006JD008268, 2007.

Xu, W., Zipser, E. J., Liu, C., and Jiang, H.: On the relationships between lightning frequency and thundercloud parameters of regional precipitation systems, J. Geophys. Res., 115, D12203, doi:10.1029/2009JD013385, 2010.

Yair, Y., Lynn, B., Price, C., Kotroni, V., Lagouvardos, K., Morin, E., Mugnai, A., and del Carmen Llasat, M.: Predicting the potential for lightning activity in Mediterranean storms based on the Weather Research and Forecasting (WRF) model dynamic and microphysical fields, J. Geophys. Res., 115, D04205, doi:10.1029/2008JD10868, 2010.

Zipser, E. J.: Deep cumulonimbus cloud systems in the tropics with and without lightning, Mon. Weather Rev., 122, 1837–1851, 1994.

Zipser, E. J. and LeMone, M. A.: Cumulonimbus Vertical Velocity Events in GATE. Part II: Synthesis and Model Core Structure, J. Atmos. Sci., 37, 2458–2469, 1980.

Zipser, E. J. and Lutz, K. R.: The vertical profile of radar reflectivity of convective cells: A strong indicator of storm intensity and lightning probability?, Mon. Weather Rev., 122, 1751–1759, 1994.

Zipser, E. J., Cecil, D. J., Liu, C., Nesbitt, S. W., and Yorty, D. P.: Where are the most intense thunderstorms on Earth? B. Am. Meteorol. Soc., 87, 1057–1071, 2006.

Zipser, E. J., Twohy, C. H., Tsay, S. C., Thornhill, K. L., Tanelli, S., Ross, R., Krishnamurti, T. N., Ji, Q., Jenkins, G., Ismail, S., Hsu, N. C., Hood, R., Heymsfield, G. M., Halverson, J., Goodman, H. M., Ferrare, R., DUNION, J. P., Douglas, M., Cifelli, R., Chen, G., Browell, E. V., and Anderson, B.: The Saharan air layer and the fate of African easterly waves – NASA's AMMA field study of tropical cyclogenesis, B. Am. Meteorol. Soc., 90, 1137–1156, 2009.